AADE-11-NTCE-72

Transient, Multiphase, Three-Dimensional Pumping Models for Cementing and Drilling

Wilson Chin and Xiaoying Zhuang, Stratamagnetic Software, LLC

Abstract

Successful pumping of multiple non-Newtonian fluids through drillpipe and up highly eccentric annuli with washouts, cuttings beds and fractures, important to cementing and drilling, is critical to optimal fluid displacement and pressure control in deepwater horizontal wells. Detailed job planning is essential, requiring solutions to transient, multiphase, non-Newtonian flow formulations written to custom, boundary-conforming, curvilinear grids, providing high physical resolution in tight annular spaces. Nonlinear momentum equations with position and species-dependent rheological properties, which number as many as there are fluids in the pumping schedule, must be solved quickly to be useful. Given their mathematical complexity, simplifying approaches are required. Existing "explicit" finite difference methods tend to be unstable numerically, and solutions can require hours-long computing and massive storage. A new approach taking advantage of the disparate physical scales underlying typical operational problems, integrating boundary-layer, self-similarity and asymptotic methods used in fluid mechanics, is described which solves the general formulation for transient, multiphase, three-dimensional flow in seconds. Examples for managed pressure drilling and cement-spacer-mud displacement are provided, emphasizing both the user interface and detailed velocity, apparent viscosity, shear rate and viscous stress fields, which automatically display in color. Analytical validations for practical applications with reciprocation and rotation are also presented. The complete transient three-dimensional problem from mudpump, through the drillpipe and borehole annulus, and finally to the return surface, is modeled.

Introduction

Non-Newtonian flows in highly eccentric annuli with cuttings beds, washouts and fractures, encountered in cementing and managed pressure (and underbalanced) drilling, are solved without crude slot flow and hydraulic radius approximations. The nonlinear partial differential equations, written to customized, boundary-conforming, curvilinear coordinate grid systems providing high physical resolution in tight spaces, are solved exactly with no-slip conditions, and detailed velocity, apparent viscosity, shear rate and viscous stress fields are computed for pressure drop, hole cleaning and other applications. For fluids with yield stress, well known uncertainties related to plug zone size and shape are fully resolved using Herschel-Bulkley relations applicable across transition boundaries (determined iteratively as part of the solution) reaching into and across the plug. Two-dimensional, single-phase, steady flow simulations, solved rapidly using finite difference methods, provide detailed numbers and color displays for all physical quantities within seconds, with excellent numerical stability for all fluid types with and without yield stress. Formulations for steady-state casing or drillpipe longitudinal translation and rotation are presented, and extensions to model transient incompressible effects associated with starting, stopping and periodic movement, important in evaluating cement-mud displacement efficiency, axial-helical cuttings transport, swab-surge, and jarring remedies for freeing stuck pipe, are developed. Practical problems are presented and the advantages over existing models are described.

In this paper, extensive calculation methods and new modeling capabilities are presented for job planning and fully transient, multiphase, three-dimensional, rotating and non-rotating flow analysis in modern managed pressure drilling and cement-mud displacement applications.

Background

Annular flow modeling in boreholes, important to both drilling and cementing, is as old as petroleum engineering itself. In the simplest case, flow configurations are represented by concentric circles through which steady, two-dimensional, Newtonian and power law fluids flow; in these limits, exact analytical or numerical solutions of the flow equations provide useful tools for operational applications. For more complicated problems, e.g., eccentric annuli, non-ideal geometric irregularities, non-Newtonian yield stress fluids, pipe translation and rotation, however, numerous mathematical obstacles arise, which unfortunately introduce inefficiencies into field practices. We discuss these problems next.

Geometric complications. In deviated and horizontal wells, heavy pipe and drill collar weight implies eccentric positioning within the borehole, as shown in (a) of Fig. 1, leading to difficulties in geometric description and solution. High eccentricities are often accompanied by non-symmetrical

washouts, thick and irregularly formed cuttings beds, and possibly, fracture indentations. Early in petroleum engineering, the notion of a simple "mean hydraulic radius" permitting representation as an equivalent circular pipe flow, as depicted in (b) of Fig. 1, was widely employed; this approach, however, was not useful since what is meant by "mean" is not obvious and certainly not generally applicable from one situation to the next. Later "slot flow" models "unwrapped" the eccentric annulus, with the result as illustrated in (c) of Fig. 1, and then, further discretized the resulting slot into local parallel plate elements, each of which is approximately modeled by simple solutions for fluid flow between ideal parallel plates. While somewhat reasonable, this approach applied strictly to very narrow annuli, but even then, curvature terms in the general governing momentum equations are always neglected. Thus, inertial effects are never properly modeled even in the limit of very narrow elements.

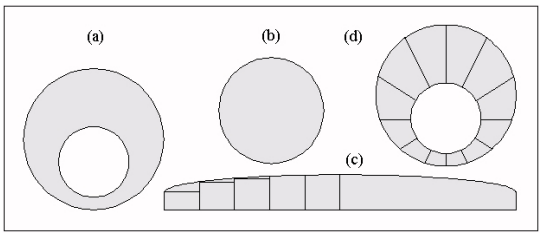

Fig. 1 – Idealizations commonly used to represent eccentric borehole annuli.

Improvements to slot flow models are provided by "pie slice" formulations, idealized in (d) of Fig. 1, in which eccentric annuli are represented by "pie slices" of varying size and included angle having the pipe center as a virtual origin. The solution for each slice is taken from the numerical solution for a concentric annular problem with a closely matched radius. In this approach, pie slices ranging from small to large are used. However, it is clear from the sketch that perfect geometric matching of the borehole boundary is never completely achieved, so that adequate modeling of curvature effects is approximate at best. Moreover, the concentric solutions used are numerical in the case of yield stress fluids and awkward in implementation. More recently, authors have used "bipolar coordinates" to represent eccentric circles, and while these provide useful host formulations for zero-yield-stress fluids, the algebra required to represent even the simplest non-Newtonian flow problems is overwhelming compared to the methods introduced later. The mapping method used in the present paper, it turns out, provides superior modeling capabilities in that the complete momentum equation for any rheology and annular geometry can be solved exactly. The new approach is less intensive numerically and easily describes realistic cuttings beds, washouts and fracture indentations.

Geometric difficulties, however, are much more than what meets the eye. When yield stress fluids flow, "plug regimes" that move as solid bodies are always present in flow domains below a given yield stress. When slot flow or pie slice models are used to simplify the solution process, "plug rings" are always obtained by virtue of the adhoc recipes described above. This is physically incorrect in most operational situations characterized by high eccentricity. For example, one would expect a large, isolated, almost circular plug element at the wide side of (a) of Fig. 1 and perhaps in a narrow strip at the bottom, but a flow containing such a solid plug would be ruled out by both solution methods. Until recently, of course, exact solutions for (a) of Fig. 1 with yield stress fluids, e.g., Bingham plastics and Herschel-Bulkley models, were impossible anyway for one important reason – theoretically, the size and shape of the plug zone are unknown in problems without azimuthal symmetry, and without knowledge of these internal boundary properties, a complete flow solution could not be obtained. This paper addresses and solves this problem in its complete generality.

Mathematical difficulties. Ideally, one would represent the details of highly eccentric annular domains exactly and in their entirety using boundary-conforming, curvilinear meshes, to which the governing equations of motion would be written, solved, and post-processed for relevant engineering information. However, this is often numerically difficult because there are as many distinct partial differential equation formulations as there are fluid rheologies, e.g., the equations for Newtonian, power law, Bingham plastic and Herschel-Bulkley fluids are very different, each with its own convergence, stability and physical properties. Moreover, because the equations are generally nonlinear, solutions must be obtained by iterative means. In fact, iterative solutions solving complicated grid generation equations must be followed by iterative solutions to produce the required flowfields on the resulting meshes. These difficulties are compounded, typically, by user inexperience in computational grid generation and numerical analysis. Even when solutions to underlying velocity fields are available, post-processed field solutions for shear rate, viscous stress, apparent viscosity, and so on, need to be automated and rapidly displayed in order to be useful in real-time applications. This requirement is particularly relevant in ultra-deepwater applications since fast and accurate pressure solutions are required to navigate the narrow window between formation fracture and disastrous blowout. These problems are all addressed in the software development program.

User interface considerations. Assuming that both geometric and mathematical issues can be addressed satisfactorily, human factors issues relating to software usage become all-important especially in anticipated applications to managed pressure drilling in ultra-deepwater drilling and hole-cleaning at high deviation angles. Physical formulations must be mathematically rigorous, numerical solutions must be detailed and pertinent to the annular geometry at hand, and complete field solutions for all engineering properties must be achievable in a manner that is completely transparent to typical engineering users with undergraduate degrees – and, even better, to field technicians with minimal modeling experience or mathematical training. This requires fully

automatic grid generation, nonlinear equation setup and stable matrix inversion.

The user interface must be designed with rigsite workflows in mind. Importantly, accuracy and speed, that is, "desktop speed" from problem definition to automated color displays, go hand-in-hand, because of demands imposed by narrow margins between pore-pressure and fracture-pressure gradient profiles in modern offshore applications. All of the above considerations, again, accurate geometric modeling, rigorous mathematical formulation and solution, and fast, user-friendly, graphically-oriented software implementation, render the general annular flow modeling problem extremely challenging. We now address each of the foregoing issues and explain how the solutions satisfactorily address these needs.

Exact Geometric and Mathematical Formulation

Boundary-conforming, curvilinear meshes. Coordinate systems "natural" to engineering problems play vital roles in facilitating efficient and accurate computational solutions. For example, circular coordinates are natural to circular wells producing from infinite reservoirs, while rectangular systems are ideal for problems solving, say, temperature distributions on rectangular plates. By the same token, a mesh system suitable for eccentric annular geometries would have inside coordinate lines that coincide with circular or square drill collars with stabilizers, while outside lines would conform to irregular borehole walls with their cuttings beds, washouts and fracture indentations. A second set of coordinate lines might be constructed orthogonally to the first, although this is not necessary if all terms in the resulting transformed governing equations are retained. By contrast, it is clear that rectangular (x,y) or circular (r,θ) coordinates are less than satisfactory for accurate geometric description of general annuli.

In natural "boundary-conforming, curvilinear coordinates," here denoted by (ξ,η), boundary conditions would be easily specified. For example, the no-slip velocity condition for stationary surfaces, say, at pipe and borehole surfaces, is simply described by "$u = 0$" along horizontal grid lines $\xi = \xi_{pipe}$ and $\xi = \xi_{borehole}$ where the subscripted numbers are constants. By contrast, the formulation in rectangular coordinates would require $u = 0$ applied along cumbersome curves, e.g., $u\{x,f(x)\} = 0$ where $y = f(x)$ represents internal and external contours.

The objective behind grid generation is a set of transformations $\xi(x,y)$ and $\eta(x,y)$ that enable simple boundary condition implementation, so that a complicated physical region, here the eccentric borehole annulus, becomes a simple rectangular one in a computational domain, where the solution of the mathematical problem is undertaken. Once the mapping transforms are available, the governing equation itself must be expressed in the new coordinates. For example, the partial differential equation for steady-state, two-dimensional, Newtonian fluid flow is the well known $u_{xx} + u_{yy} = - \mu^{-1} \partial P/\partial z$ where μ and $\partial P/\partial z$ represent viscosity and applied pressure gradient. Although this appears in rectangular coordinates, the equation applies to all annular geometries.

The conversion process itself is straightforward. Suppose we wish to express a function $u(x,y)$ in terms of convenient independent variables ξ and η. If the transformations $x = x(\xi,\eta)$ and $y = y(\xi,\eta)$ are available, direct substitution allows us to rewrite $u(x,y)$ in the form $u(x,y) = U(\xi,\eta)$, where the functional relation $U(\xi,\eta)$ between ξ and η is generally different from the relation $u(x,y)$ connecting x and y. Derivatives of $u(x,y)$ with respect to x and y are easily related to derivatives of $U(\xi,\eta)$ taken with respect to ξ and η. For example, it is easily shown that $U_\xi = u_x x_\xi + u_y y_\xi$ and $U_\eta = u_x x_\eta + u_y y_\eta$ for the first derivatives, with obvious extensions to second derivatives obtained using the chain rule of calculus. In general fluid-dynamical problems, the resulting equation for $U(\xi,\eta)$ is typically more complicated than that for $u(x,y)$. The computational benefit, however, is accurate and noise-free implementation of boundary conditions, not to mention the use of much fewer grid points for the same level of physical resolution. Calculated solutions are displayed in physical space with the assistance of custom color plotting routines.

Many commercial simulators calculate velocities and other flow properties directly using rectangular (x,y) grids. We emphasize that x-y coordinate lines do not conform to the irregular curves defining near and farfield boundaries; also, high grid densities imposed, say at the bottom of an eccentric annulus, would require similarly high densities far away where detailed resolution is unnecessary. This results in large, inefficient computing domains containing dead flow and extremely large matrices. In addition, "choppy" meshes lead to noise, inaccuracy and instability. Other simulators, particularly general purpose codes used in computational fluid dynamics (CFD), do support automatic and efficient "finite element" or "finite volume" gridding. However, they are not portable in the sense that special licenses must be purchased for users, thus incurring significant costs. But more importantly, they run proprietary, high-overhead "canned" routines that cannot be adapted to new mathematical models (such as the novel yield stress formulation introduced below) and cannot be "tuned" to run optimally. Also, they offer inflexible output formats that are not easily integrated with custom designed graphics and user interface software. In this paper, the objective is a fast, flexible and accurate solution procedure that can be installed on all operating systems at minimal cost.

We conceptually describe the grid generation process in this paper. Details are offered in the principal author's books on drilling and reservoir engineering, e.g., see Chin (1992, 2001, 2002). We reiterate the basic ideas here because they are essential to understanding the solution approach and its topological advantages. Rather than dealing directly with $\xi = \xi(x,y)$ and $\eta = \eta(x,y)$, we equivalently consider the inverse functions $x = x(\xi,\eta)$ and $y = y(\xi,\eta)$ satisfying *nonlinear* coupled partial differential equations, which are derived in the form

$$(x_\eta^2 + y_\eta^2)\, x_{\xi\xi} - 2\,(x_\xi x_\eta + y_\xi y_\eta)\, x_{\xi\eta} + (x_\xi^2 + y_\xi^2)\, x_{\eta\eta} = 0 \quad (1)$$

$$(x_\eta^2 + y_\eta^2)\, y_{\xi\xi} - 2\,(x_\xi x_\eta + y_\xi y_\eta)\, y_{\xi\eta} + (x_\xi^2 + y_\xi^2)\, y_{\eta\eta} = 0 \quad (2)$$

where ξ and η are now independent (as opposed to dependent) variables. We aim to map the irregular flow domain of Fig. 2a into the simple rectangular computational domain of Fig. 2b where B_1 and B_2 are physically insignificant "branch cuts" where single-valued solution constraints are enforced.

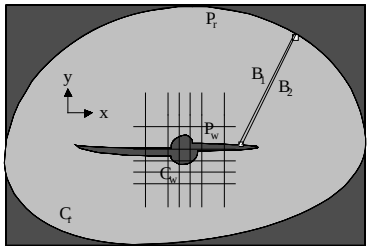

Fig. 2a – Irregular physical domain with inefficient rectangular meshes.

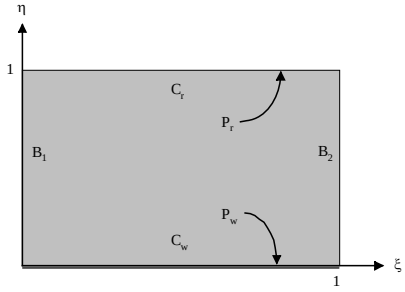

Fig. 2b – Irregular domain mapped to rectangular computational space.

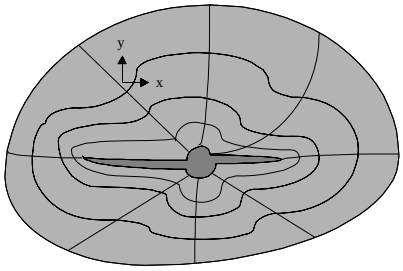

Fig. 2c – Physical domain in boundary-conforming coordinates.

How are the foregoing equations used to create numerical mappings? Suppose that contour C_W in Fig. 2a is to map into η = 0 of Fig. 2b. The user first discretizes C_W in Fig. 2a by penciling along it a sequence of dots chosen to represent the curve. If these are selected in an orderly, say, clockwise fashion, they define the direction in which ξ increases. Along η = 0, values of x and y are known (e.g., from measurement on graph paper) as functions of ξ . Similarly, x and y values along C_r are known as functions of ξ on η = 1 of Fig. 2b. These provide the boundary conditions for Eqs. 1 and 2, which are augmented by single-valuedness constraints at arbitrarily chosen branch cuts B_1 and B_2. It is clear that this process is easily automated by computer.

Conventionally, in grid generation, Eqs. 1 and 2 are discretized by finite differences and solved by point or line relaxation, starting with guesses for the dependent variables x and y. The problem is linearized by approximating all nonlinear coefficients using values from earlier iterations. Typically, several updates to Eq. 1 are taken, followed by updates to Eq. 2, with this cycling process, often unstable, repeated continuously until convergence. Variations of the approach are known, with 100 × 100 mesh systems in the ξ-η plane requiring minutes of computing time. Once x = x(ξ,η) and y = y(ξ,η) are solved and tabulated as functions of ξ and η, physical coordinates are generated. First, η is fixed; for each node ξ along this η, computed values of (x,y) pairs are successively plotted in the x-y plane to produce the required closed contour. This procedure is repeated for all values of η, until the entire family of closed curves is obtained, with limit values η = 0 and η = 1 again describing C_w and C_r. Orthogonals are constructed by repeating the procedure, with η and ξ roles reversed.

This process provides the curvilinear mapping only. The equation describing the physics (e.g., the Navier-Stokes equation for Newtonian flow or the general rheological equations for non-Newtonian fluids) must be transformed into (ξ,η) coordinates and solved. In general, the transformed governing equation, which is algebraically more complicated, must be solved, and this procedure introduces its own complications and numerical challenges. The "simplification," however, lies not in the transformed equation, which now contains mixed derivatives and variable coefficients, but in the computational domain itself, because this domain takes on a rectangular form amenable to simple, noise-free numerical solution, requiring significantly fewer nodal points for high resolution physical definition.

Again, existing solution methods solving x(ξ,η) and y(ξ,η) stagger the solutions for Eqs. 1 and 2. For example, crude solutions are used to initialize the coefficients of Eq. 1, and improvements to x(ξ,η) are obtained. These are used to evaluate the coefficients of Eq. 2, in order to obtain an improved y(ξ,η); then, attention turns to Eq. 1 again, and so on, until convergence is achieved. Various over-relaxation means are used to implement these iterations, e.g., point SOR, line SLOR, line SOR with explicit damping, alternating-direction-implicit, and multigrid, with varying degrees of success. Often these schemes diverge computationally. In any event, the staggering used introduces different artificial time levels while iterating. Classic numerical analysis, however, suggests that faster convergence and improved stability are possible by reducing the number of time levels.

A new approach to rapidly solve the nonlinear coupled grid generation equations was proposed by the principal author a decade ago and is based on a very simple idea. This idea has since been validated in numerous applications. Consider first $z_{\xi\xi} + z_{\eta\eta} = 0$, for which $z_{i,j} \approx (z_{i-1,j} + z_{i+1,j} + z_{i,j-1} + z_{i,j+1})/4$ holds on constant grid systems (this is easily derived using standard finite difference formulas). This well-known averaging law motivates the *recursion formula* $z_{i,j}^{n} = (z_{i-1,j}^{n-1} + z_{i+1,j}^{n-1} + z_{i,j-1}^{n-1} + z_{i,j+1}^{n-1})/4$ often used to illustrate and develop multilevel iterative solutions; an approximate, and even trivial solution, can be used to initialize

the calculations, and nonzero solutions are always produced from nonzero boundary conditions.

But the well-known Gauss-Seidel method is fastest: as soon as a new value of $z_{i,j}$ is calculated, its previous value is discarded and overwritten by the new value. This speed is accompanied by low memory requirements, since there is no need to store both n and n-1 level solutions: only a single array, $z_{i,j}$ itself, is required in programming. The approach to Eqs. 1 and 2 was motivated by the following idea. Rather than solving for $x(\xi,\eta)$ and $y(\xi,\eta)$ in a staggered, leap-frog manner, is it possible to *simultaneously* update x and y in a similar once-only manner? Are convergence rates significantly increased? What formalism permits us to solve in Gauss-Seidel fashion? What are the programming implications?

Complex variables are used often in harmonic analysis problems; for example, the real and imaginary parts of an analytical function f(z), where $z = x + i\,y$, provide solutions satisfying Laplace's equation. Here we use complex analysis differently. We *define* a dependent variable z by $z(\xi,\eta) = x(\xi,\eta) + i\,y(\xi,\eta)$, and then add Eq. 1 plus *i* times Eq. 2, in order to obtain the net result $(x_\eta^2 + y_\eta^2)\, z_{\xi\xi} - 2\,(x_\xi x_\eta + y_\xi y_\eta)\, z_{\xi\eta} + (x_\xi^2 + y_\xi^2)\, z_{\eta\eta} = 0$. Now, the complex conjugate of z is $z^*(\xi,\eta) = x(\xi,\eta) - i\,y(\xi,\eta)$, from which we find that $x = (z + z^*)/2$ and $y = -\,i\,(z - z^*)/2$. Substitution produces the simple and equivalent one-equation result

$$(z_\eta z_\eta^*)\, z_{\xi\xi} - (z_\xi z_\eta^* + z_\xi^* z_\eta)\, z_{\xi\eta} + (z_\xi z_\xi^*)\, z_{\eta\eta} = 0 \quad (3)$$

This form yields significant advantages. First, when z is declared as a complex variable in a Fortran program, Eq. 3 represents, for all practical purposes, a *single* equation in $z(\xi,\eta)$. There is no need to leap-frog between x and y solutions now, since a single formula analogous to the classical model $z_{i,j} = (z_{i-1,j} + z_{i+1,j} + z_{i,j-1} + z_{i,j+1})/4$ is easily written for the $z_{i,j}$ using Eq. 3 as the host equation. Because both x and y are simultaneously resident in computer memory, the extra time level present in staggered schemes is completely eliminated, as in the Gauss-Seidel method. In thousands of test simulations conducted using point and line relaxation, convergence times are shorter by orders of magnitude relative to those obtained for cyclic solution between $x(\xi,\eta)$ and $y(\xi,\eta)$. Convergence appears to be unconditional, monotonic and stable. Because Eq. 3 is nonlinear, von Neumann tests for exponential stability and traditional estimates for convergence rate do not apply, but the evidence for stability and convergence, while empirical, remains very strong and convincing since we have always computed useful grids in all test runs.

Iterative solution of nonlinear partial differential equations. Earlier we noted that $u_{xx} + u_{yy} = -\,\mu^{-1}\,\partial P/\partial z$ applies to steady, two-dimensional, single-phase Newtonian flows for borehole annuli having the most complicated shapes; unfortunately, practical solutions cannot be accurately obtained in (x,y) coordinates. Here, μ is a constant viscosity and $\partial P/\partial z$ is the applied pressure gradient in the z direction assumed to be known. This is the so-called Poisson equation in mathematics, and students who have undertaken its study realize that, despite the apparent simplicity offered by few terms and complete linearity, useful solutions to the classical model are nonetheless difficult to obtain. When the underlying fluid is nonlinear, this equation is replaced by Eq. 4, which is vastly more complicated, that is,

$$\partial\,(N\,\partial u/\partial y)/\,\partial y \;+\; \partial\,(N\,\partial u/\partial x)/\,\partial x \;=\; \partial P/\partial z \quad (4)$$

where N now represents the "apparent viscosity" function. This apparent viscosity is not constant, but a function of local shear rates whose mathematical form depends on the particular rheology assumed. For example, in the case of power law fluids modeled by an exponent "n" and a consistency factor "K," N takes the form $N = K\,[\,(\partial u/\partial y)^2 + (\partial u/\partial x)^2\,]^{(n-1)/2}$. Even without solving the problem, it is clear that, since $\partial u/\partial x$ and $\partial u/\partial y$ depend on the (unknown) solution itself, any resulting apparent viscosity must vary locally within the flow domain and depend on both geometric details and flow rate. Detailed computed solutions for annular flows are presented in Chin (1992, 2001) where approximate approaches to plug flow modeling are used.

Because Eq. 4 is now strongly nonlinear, the solution process at its very heart must remain nonlinear. This implies that one cannot use simpler Newtonian solutions as leading approximations and focus on higher order improvements to them. The basic solution method must retain a fully nonlinear character in order that well known nonlinear relationships between pressure gradient and volume flow rate evolve as part of an iterative computational process. As if this alone were not complicated enough, we emphasize that it is the re-expression of Eq. 4 in general (ξ,η) curvilinear coordinates, not in simple (x,y) coordinates, that must be solved, and that these coordinates and their metrics are only available numerically.

The transformed equation now contains additional terms as well as nonlinear coefficients that depend on the mapping. Direct solutions are not numerically possible, but exact solutions can be obtained iteratively. In fact, finite difference methods are used; the solutions are obtained line-by-line using so-called "successive line over relaxation" (SLOR) schemes written in the curvilinear coordinates. These iterative solutions are initialized by "close" analytical or numerical solutions; the closer the initial guess, the more rapid the convergence. For typical problems, the efficient schemes devised will produce a usable curvilinear grid in approximately one second of computing time, while the solution of the transformed momentum equation (when pressure gradient is specified) may require two-to-three seconds. Again, detailed discussions and computed solutions for power law and simple plug flows in highly eccentric annuli, with practical applications, are given in Chin (1992, 2001). The approximate plug flow methods developed in these early researches are now obsolete and are replaced by the following exact approach for yield stress description and modeling.

Yield stress, plug zone size and shape modeling. In fluid flows where yield stresses exist, "plug zones" are to be

found. These plugs move as solid bodies within the flowing system. For pipes with circular cross-sections and for concentric annuli, it is possible to derive exact analytical solutions for plug zone size and shape for Bingham plastics (general solutions have, in fact, been derived for both geometries assuming Herschel-Bulkley fluids, and will be presented separately). For circular pipes, the cross-sectional plug is simply a circle; for concentric annuli, of course, the plug is a concentric ring.

The appearance of solid plugs within moving streams results from the rheological model used by mathematicians to idealize the physics. If we denote the shear rate functional by $\Gamma = [\ (\partial u/\partial y)^2 + (\partial u/\partial x)^2\ ]^{1/2}$, this idealization can be written formally as

$$N = k\,\Gamma^{n-1} + S_{yield}/\Gamma \text{ if } \{1/2 \text{ trace } (\underline{\mathbf{S}}\bullet\underline{\mathbf{S}})\}^{1/2} > \tau_0$$
$$\underline{\mathbf{D}} = 0 \text{ if } \{1/2 \text{ trace } (\underline{\mathbf{S}}\bullet\underline{\mathbf{S}})\}^{1/2} < \tau_0 \qquad (5)$$

where the general extra stress tensor is denoted by $\underline{\mathbf{S}}$ and the deformation tensor is given by $\underline{\mathbf{D}}$. Here, τ_0 is the so-called "yield stress." The discontinuous "if, then" character behind Eq. 5 is responsible for the sudden transition from shear flow to plug flow commonly quoted. As noted, for flows with azimuthal symmetry, that is, circular pipes and concentric annuli, exact, rigorous mathematical solutions are in fact possible.

For non-circular ducts and eccentric annuli, which describe a large number of practical engineering problems, it has not been possible to characterize plug zone size and shape, even approximately. Thus, the most significant petroleum engineering flow problems important to both drilling and cementing cannot be modeled at all, let alone accurately. In order to remedy this situation, we observe that the discontinuity offered in Eq. 5 is really an artificial one, introduced for, of all reasons, "simplicity." This unfortunately leads to the solution difficulties noted. In reality, practical engineering flows do not suddenly turn from shear to plug flow; the transition may be rapid, but it will occur continuously over finite measurable distances. We therefore turn to more realistic rheological models which apply continuously throughout the *entire* problem domain, and which, if the underlying flow parameters permit, lead to plug zones naturally during the solution process.

The conventional Herschel-Bulkley viscoplastic model, which includes Bingham plastics as a special limit when the exponent "n" is unity, requires that $\tau = \tau_0 + K(d\gamma/dt)^n$, if $\tau > \tau_0$ and $d\gamma/dt = 0$ otherwise. Here τ is the shear stress, τ_0 is the yield stress, K is the consistency factor, n is the exponent, and $d\gamma/dt$ is the shear rate. As explained, this model is far from perfect. For example, both Herschel-Bulkley and Bingham plastic models predict infinite viscosities in the limit of vanishing shear rate, a fact that often leads to numerical instabilities. In addition, the behavior is not compatible with conservation laws that govern many complex flows.

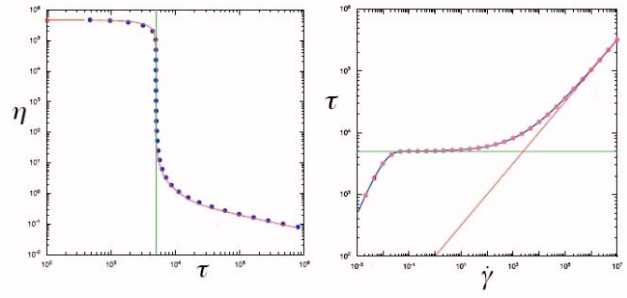

Fig. 3 – Extended Herschel-Bulkley law.

An alternative to the standard Herschel-Bulkley model is the use of continuous functions which apply to sheared regimes, and in addition, through and into the plug zone. One such example model is suggested by Souza, Mendez and Dutra (2004), that is, $\tau = \{1 - \exp(-\eta_0\, d\gamma/dt\ /\tau_0)\}\{\tau_0 + K(d\gamma/dt)^n\}$, which would apply *everywhere* in the problem domain. The corresponding apparent viscosity N, for numerical implementation in Eq. 4, is denoted by

$$\eta = \tau\ /(d\gamma\ /dt)$$
$$= \{1 - \exp(-\eta_0\, d\gamma/dt\ /\tau_0)\}\{\tau_0/(d\gamma/dt) + K(d\gamma/dt)^{n-1}\} \qquad (6)$$

The "apparent viscosity vs shear stress" and "shear stress vs shear rate" diagrams, from Souza *et al*, are duplicated in Fig. 3. What are the physical consequences of this model? Eq. 6, in fact, represents an "extended Herschel-Bulkley" model in the following sense. For infinite shear rates, one would recover $\tau = \tau_0 + K(d\gamma/dt)^n$. But for low shear rates, a simple Taylor expansion leads to $\eta \approx \{\eta_0(d\gamma/dt)\ /\tau_0\}\{\tau_0/(d\gamma/dt) + K(d\gamma/dt)^{n-1}\} \approx \eta_0$ where it is clear now that η_0 represents a very high viscosity for the plug zone. The use of Eq. 6 in numerical algorithms simplifies both formulation and coding since internal boundaries and plug domains do not need to be determined as part of the solution. A single constitutive law (as opposed to the use of two relationships in Eq. 5) applies everywhere, thus simplifying computational logic; moreover, the continuous function assumed also possesses continuous derivatives everywhere and allows the use of standard difference formulas. Cumbersome numerical matching across internal boundaries is completely avoided. In a practical computer program, the plug zone viscosity might be assumed, for example, as 1,000 cp. In fact, we choose high values of η_0 which would additionally stabilize the numerical integration schemes used. This strategy is applied throughout this work, both to the iterative relaxation schemes for steady-state problems and to the transient integration schemes for more complicated formulations. This new approach was first discussed in Chin and Zhuang (2010) for steady flows and has since been incorporated in the fully transient annular flow modeling approaches.

Borehole axis radius of curvature. Borehole axis curvature is important to ultra-deepwater drilling, especially in short and medium radius turning applications. Several aspects of cuttings transport and debris removal are not completely understood insofar as centrifugal effects are concerned and a

study of curvature effects contributes to an understanding of their influence on stress fields. Also, bends in pipelines and annuli are interesting because they are associated with losses; that is, to maintain a prescribed volume flow rate, a greater pressure drop is required in pipes with bends than those without. This is true because the viscous stresses acting along pipe walls are higher. The modeling of borehole axis curvature effects for problems involving noncircular ducts and highly eccentric annuli containing non-Newtonian fluids was first addressed in Chin (2001), where detailed derivations, equations and computed examples are given. Essentially, it is shown how, by replacing "$1/\mu \quad \partial P/\partial z$" with an inertially corrected "$1/\mu \quad \partial P/\partial z - 1/R \; \partial u/\partial r + u/R^2$" where R is the radius of curvature, the effective pressure gradient accounting for centrifugal effects is properly and stably modeled. This model is incorporated into Eq. 4 and a radius of curvature entry appears in the software menu in Fig. 4a at the bottom left.

Single-Phase Steady and Transient Formulations: User Interface and Physical Modeling Capabilities

Simulators for two-dimensional steady and transient flow are described in this paper, applicable to single-phase, Herschel-Bulkley fluids, which may also be operated in Newtonian, power law and Bingham plastic modes. For Bingham plastic and Herschel-Bulkley fluids, the generalized rheological approach is used and plug zone sizes and shapes are determined automatically whatever the eccentric annular geometry. The intuitive user interface shown in Fig. 4a requires only an elementary understanding of engineering vocabulary and the simulator may be operated with minimal training. Annular geometry is defined by entering center coordinates and radii in the upper left menu. Clicking 'Show Annulus' provides an instantaneous display of the geometry assumed, plus a typical curvilinear grid, e.g., as illustrated in Fig. 4b, whose mesh density may be coarsened or refined at run-time. In addition, online editing utilities allow the baseline eccentric circles to be edited for washout, cuttings bed or fracture modification effects.

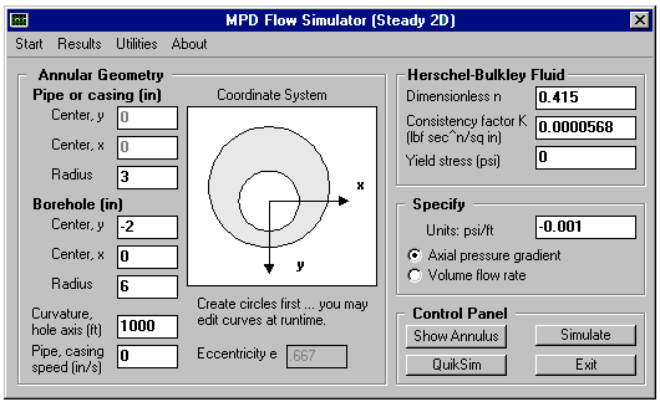

Fig. 4a – Steady flow user interface.

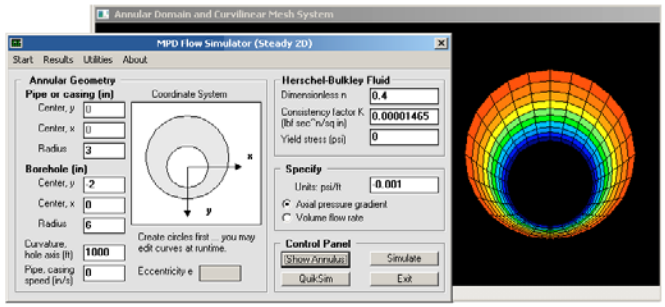

Fig. 4b – Quick annular geometry and curvilinear grid display mode.

Rheological parameters for the general Herschel-Bulkley fluid are entered into the input boxes at the upper right of Fig. 4a. Four model are possible by choosing the values of n, K and τ_0 appropriately. Newtonian fluids require n = 1 and τ_0 = 0, while power law fluids allow general n with vanishing τ_0. On the other hand, Bingham plastics require n = 1 and non-vanishing τ_0, while all three parameters may be generally assumed in the case of Herschel-Bulkley fluids. Fig. 4c also shows two utilities for n and K determination in the case of power law fluids, that is, assuming Fann dial readings or viscosity and shear rate data are available.

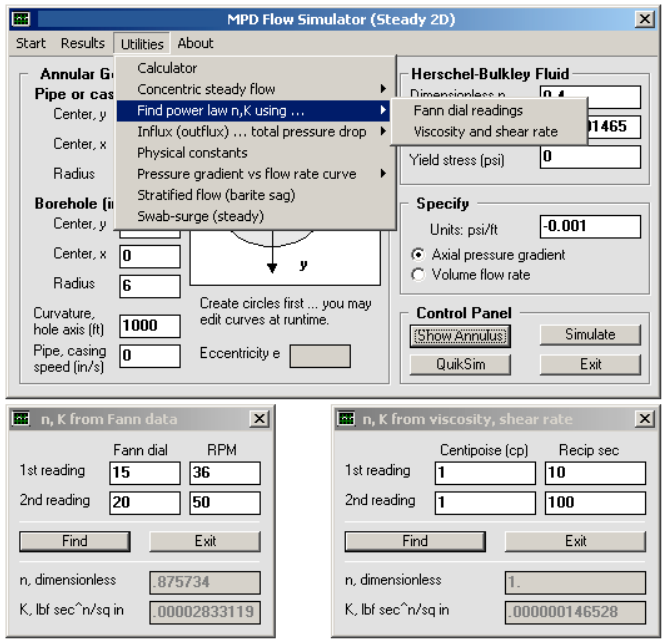

Fig. 4c – Determining n and K for power law fluids.

It is clear from Figs. 4a – 4c that several important auxiliary capabilities have been built into the overall algorithm. First, the axis of the borehole need not be straight; it may be curved, with any constant value for radius of curvature, to model short, medium and large radius turning of the borehole in offshore applications. This properly accounts for centrifugal effects which will affect the relationship between pressure gradient and volume flow rate.

Second, the drillpipe may move in either direction relative to the borehole, that is, constant speed translational motion is permitted. In the simplest application, the drillstring penetrates the formation, moves relative to the borehole at constant positive or negative speed, and induces a purely two-dimensional flow everywhere; the value of this speed is entered into the bottom left input box of Fig. 4a. This capability also supports steady-state swab-surge analysis, with the mudpumps turned off or on and continuously running, as will be illustrated in examples later. A simple 'Worksheet' is loaded by clicking 'Swab-surge (steady)' in Fig. 4c, which prompts the user for tripping mode and speed. The positive or negative induced volume flow rate is calculated and added to the flow rate specified at the mud pump. Two calculation modes described in the next paragraph was developed for swab-surge and other drilling and cementing applications.

The option boxes immediately above the 'Control Panel' in Fig. 4a show how two computational modes are supported. In the first, the applied axial pressure gradient is specified and volume flow rate (together with detailed field solutions for all physical properties) is calculated. In the second, volume flow rate is specified and pressure gradient (together with all field properties again) is determined iteratively. The algorithm involves some subtlety because, as will be described in the application for swab-surge, the directions for drillpipe motion and net volume flow rate need not be correlated. For the "flow rate specified" mode, an initial pressure gradient is assumed for which a test rate is calculated and compared against the target rate; if the results do not satisfy a tolerance of 1%, a half-step correction procedure is applied to the test gradient and the calculations are repeated to convergence. Typically, the "pressure gradient specified" mode requires 2-3 seconds or less for a complete solution, while the "flow rate specified" mode may require up to ten seconds.

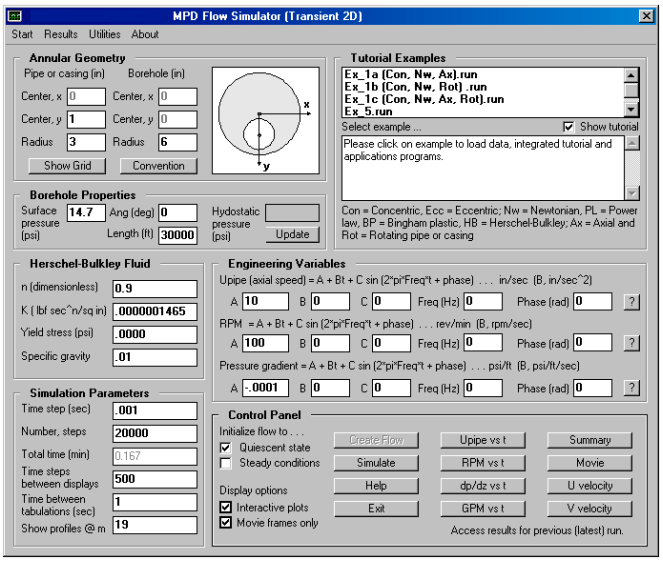

Fig. 4d – Transient flow user interface.

The foregoing remarks, focusing on the screen shot in Fig. 4a, apply to the steady flow simulator. The corresponding user interface for transient incompressible flow is shown in Fig. 4d. Now, instead of Eq. 4, fully unsteady effects are computed from its transient extension, but rewritten in custom curvilinear coordinates applicable to the particular geometry under consideration. The above menu contains similar geometry and rheology definition modules, however, general, coupled, transient functions for pipe or casing axial reciprocation, inner circle rotation and pressure gradient are permitted. Additional input boxes for time step selection to facilitate numerical time integration are shown. Importantly, a database of prior runs is offered for user convenience and education. Clicking on a named entry at the top right of Fig. 4d automatically fills in all relevant input boxes and launches any sub-applications programs that are required. Users may edit numerical values and re-run any simulations available in the database. Also, all graphical capabilities described in this paper for steady flow are also available for unsteady flows.

Color displays of engineering properties. In order to make the mathematical models useful, every effort was expended to automate the display of important field quantities using two and three-dimensional color graphics. Use of the presentation tools is completely transparent to the engineer. An 'Install Graphics' button installs all required software quickly in a single pass; in addition, user training in operating the integrated graphical capabilities is not required. On convergence of the solution, a message box (supplemented with speech output and suggestions) summarizes basic pressure gradient and flow rate relationships.

The menu in Fig. 5a indicates that text output and color displays for different physical quantities are available for display. These quantities are post-processed from the velocity solution and made available for important engineering reasons. For example, Chin (1992, 2001) shows that apparent viscosity is vital to evaluating spotting fluid effectiveness in freeing stuck pipe. On the other hand, viscous stress (at the cuttings bed) is important to studying hole cleaning in horizontal and deviated wells, while velocity and viscosity play dominant roles in vertical well cuttings transport. A complete discussion, together with validations from a number of experimental investigations, is offered in the the books by Chin (1992, 2001).

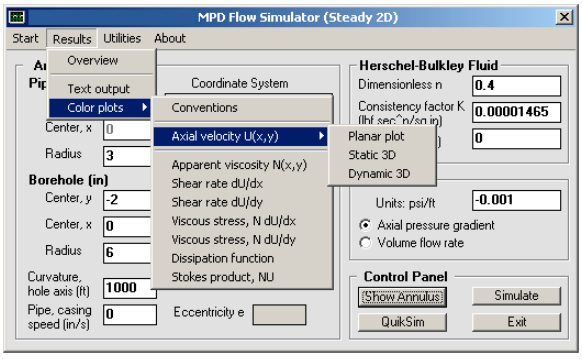

Fig. 5a – Graphical solution display options.

Fig. 5b displays results for axial velocity, apparent viscosity, shear rate, viscous stress, dissipation function and Stokes product in simple "planar plots." For the all-important velocity results, additional displays using three-dimensional color capabilities are offered as indicated in Fig. 5c. These capabilities, which include contour plots and mouse-rotatable perspective displays, are available for all mesh combinations, ranging from coarse to fine, selected by the user at run-time. These tools, plus text output, are useful in supporting detailed report generation.

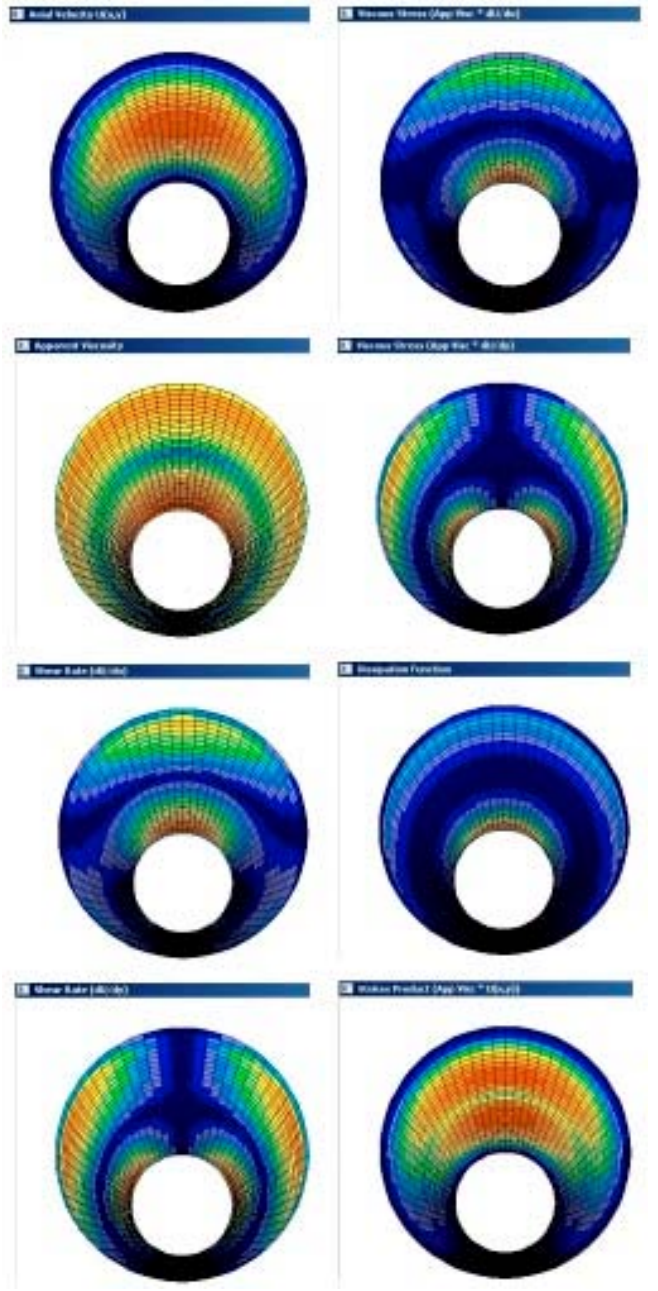

Fig. 5b – Planar color displays of key physical field quantities.

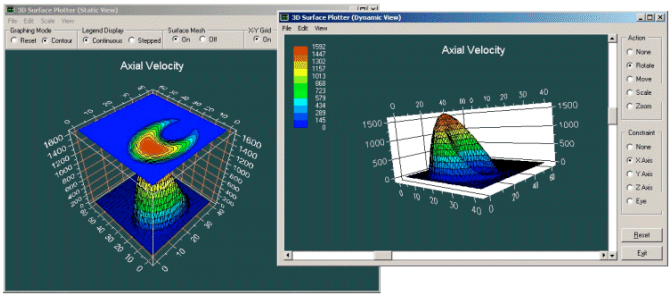

Fig. 5c – Three-dimensional, color displays (contour maps and mouse-rotatable perspective views).

Modeling borehole geometric irregularities. For convenience, the main input screen in Fig. 4a accepts off-centered circles only. When center coordinates and radii are entered for inner and outer circles, an information box displays the calculated value for dimensionless eccentricity, to provide a useful reference point for drilling applications. Built-in error checking prevents circle cross-overs. At run-time, both inner and outer circle coordinates may be changed at the user's option. As shown in Fig. 6a below, existing contour coordinates are displayed, which may be modified without restriction. The changes elected for the example shown invoke changes to seven points only, in order to describe a simple washout; this convenient online editing tool can be used to draw washouts, cuttings beds and fracture indentations of any shape. While Fig. 6a provides a simple "planar plot" of velocity, Fig. 6b provides more detailed three-dimensional resolution. Interestingly, for the simulation shown, the presence of the washout allows a 30% increase in flow rate for the same pressure gradient. General conclusions are not possible, and appropriate results must be made on a case-by-case basis.

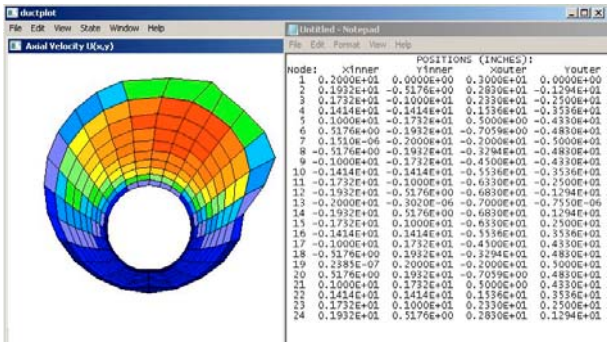

Fig. 6a – Modifying eccentric circle at run-time for washouts.

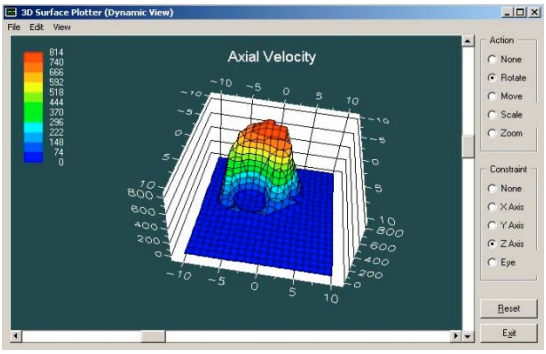

Fig. 6b – Color display of velocity field with washout.

Yield stress modeling. As noted earlier, yield stress modeling in eccentric annuli is important to both drilling and cementing applications. The use of the generalized Herschel-Bulkley constitutive model correctly predicts plug zone size and shape for all geometries. Because a continuous flow model is used, which guides the evolution of a single continuous velocity field, the computational difficulties associated with distinct internal boundaries and infinite viscosities are avoided. The method, we emphasize, will predict realistic plug zones with rapid gradients when they exist, as shown in Fig. 7a.

More interesting results are shown in Fig. 7b, in which plug zones for (1) a stationary pipe, (2) a pipe moving opposite to the direction of net flow, and (3) a pipe moving in the same direction of the main flow, are shown. Such computations are important in swab-surge applications and accurate pressure modeling. Plug zones associated with yield stress, of course, are important to understanding cuttings transport in drilling and fluid mixing in cementing. Again, no special procedures are required on the part of the user, as all dynamical features are computed automatically for both yield stress and non-yield fluids. Computation of plug zone flows requires no additional effort in terms of processing time and memory resources.

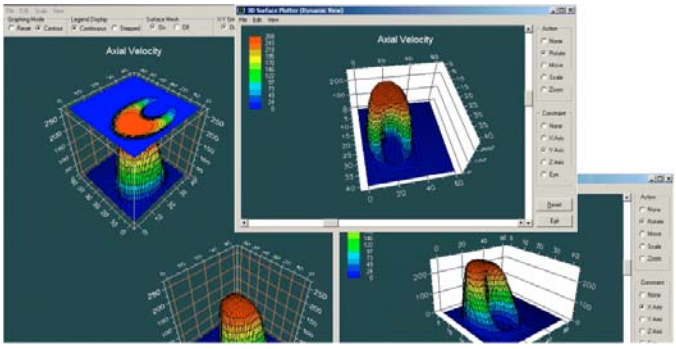

Fig. 7a – Typical velocity results for eccentric annulus with plug flow.

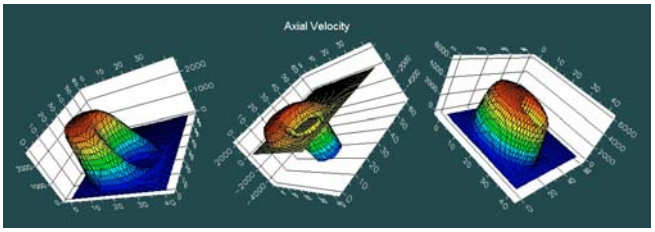

Fig. 7b – Non-Newtonian plug flow velocity profiles with stationary pipe (left), pipe moving opposite to flow (middle), and pipe moving with flow (right).

GENERAL MULTIPHASE FORMULATION

Theory, Numerical Solution and Applications

The flow of multiple non-Newtonian fluids pumped under a general schedule, allowing full borehole eccentricity, is of interest to both drilling and cementing operations. For example, in modern "managed pressure drilling" (MPD) applications, the pressure profile along the borehole wall (and, in particular, at the drillbit) as a function of time is extremely important from both safety and reservoir damage perspectives. This time-varying profile depends on the pump schedule, the rheology of the fluids being pumped, and also on the details of the annular geometry. On the other hand, in cementing operations, engineers need to monitor how mud, spacer and cement interfaces evolve over time during a cement job. Fluid intermingling may inhibit the ability of a fluid to perform its intended purpose. Good interface modeling allows operators to predict the causes of cement contamination and mud channeling before they occur in real wells. Because these two objectives are extremely important and affect safety and economic success or failure, it is extremely important to develop and implement mathematical models of the underlying phenomena having the highest scientific integrity.

Over the years, the first author has been associated with a number of leading edge research and industrial efforts aimed at solving the extremely difficult problems described in the introductory remarks on Pages 1-10. Progress in these areas has been extremely rapid. As the present paper describes new advances made during 2009-2011 in studying transient, multiphase, three-dimensional pumping models for cementing and drilling, it is important to explain the differences between the present and earlier work so that formulation and semantic differences are clearly delineated. The explanations provided here are carefully drawn only from information publicly available in published papers and product brochures.

Pre-existing 2001-2009 work. While "pre-existing" might connote work performed decades ago, we, in fact, refer to methods developed in the past ten years prior to the publication of the present paper. First we consider basic rheology models. A "Generalized Herschel Bulkley" (GHB) model was first disclosed in Becker, Morgan, Chin and Griffith (2003) which extends the Newtonian, power law, Bingham plastic and Herschel-Bulkley constitutive equation models used in the petroleum literature. In that paper, the model is given by $(\tau/\tau_{ref})^m = (\tau_0/\tau_{ref})^m + \{\mu\,(d\gamma/dt)/\tau_{ref}\}^n$ where

τ_{ref} is a reference value, τ_0 is the yield stress, μ is a viscosity and $d\gamma/dt$ is the shear rate. It is clear that, by suitable choices of the exponents m and n, the prior models are recovered. This model, like earlier models, does not apply in the plug zone, and particularly, in the transition zone separating plug and shear regimes. Thus, while it offers superior capabilities in modeling constitutive relations, it cannot be used to naturally compute flows in the entire annular domain as we have by using the "extended Herschel-Bulkley" law, i.e.,

$$\eta = \tau /(d\gamma /dt)$$
$$= \{1 - \exp(-\eta_0\, d\gamma/dt /\tau_0)\}\{\tau_0/(d\gamma/dt) + K\,(d\gamma/dt)^{n-1}\} \qquad (6)$$

Thus, the "Generalized . . ." and "extended Herschel-Bulkley" models are completely different, both in form and in purpose. The earlier model contains "m" and "n" exponents for curve-fitting and regression analysis; the present one does not. On the other hand, the earlier model cannot be used to determine the entire flowfield because the size, shape and location of any plug zones in general eccentric annuli are not known *a priori*. However, the present model predicts all of these quantities quickly and naturally.

We do note that Becker *et al* (2003) refers to the "exact numerical simulator" used in the first author's book in Chin (2001) to calculate annular flow details. While the work was "exact" at the time, the model is, in fact, now obsolete and no longer used here to model plug zones. The examples in Figs. 7a and 7b, for instance, were all calculated rigorously using the approach developed for Eq. 6 above. The prior Chin (2001) method, in retrospect, is deficient for the following reasons. Quoting from the 2001 book,

"Finally, we return to fluids with non-zero yield stresses. In general, there may exist internal boundaries separating "dead" (or "plug") and "shear" flow regimes. These unknown boundaries must be obtained as part of the solution. In free surface theory for water waves, or in shock-fitting methods for gasdynamic discontinuities, explicit equations are written for the boundary curve and solved with the full equations. These approaches are complicated. Instead, the "shock capturing" method for transonic flows with embedded discontinuities was used to capture these zones naturally during iterations. The conditions in Equations 2-14b,c [see 2001 book] were added to the "zero yield" code. This entailed tedious "point by point" testing during the computations, where the inequalities were evaluated with latest available solutions."

The "shock capturing" methods alluded to were 1970s vintage methods used in computational fluid methods to model internal discontinuities in fluid flows. For example, in aerodynamics, they *did* at first predict shockwaves, but mass was *not* conserved across shocks. Engineers nonetheless accepted the results because they fortuitously modeled the local boundary layer separation that occurs at the foot of the shock near the airfoil surface – but, from a conceptual perspective, simple shock capturing is incorrect (in aerospace engineering, this difficulty has been successfully resolved).

The shock capturing in Chin (2001) was aimed only at providing *any* computational solution that was convergent and which led to plug zones. The procedure, defined by a numerical recipe only, was never justified physically and its correctness was never established. For this reason, the first author turned his focus to embedding Eq. 6 within the framework of the curvilinear grid formulation. For years, numerical instabilities were encountered until they were successfully addressed in Chin and Zhuang (2010).

The above discussion focuses on constitutive models and their ability (or lack of) in calculating flows with plug zones. Now we turn to the calculation of fluid interfaces and the mixing that occurs there. Again, the first author helped develop the physical and mathematical models reported in References 7, 10, 11, 12 and 13, where the basic equations are given and their results compared successfully against experiment. The formulations developed are somewhat similar to Equations 9-5-1 and 9-5-2 below, except that the newer models incorporate finite difference changes needed to render Eq. 6 numerically stable and to enhance the robustness of the coupled model for rotating pipe. The 2007-2008 models predict interfaces and mixing zone properties naturally as time integrations progressed, although only to the extent possible with the limiting GHB model.

While correct, the calculations can be extremely time-consuming, especially if the method is generalized to handle multiple fluid species as suggested in a 2008 product brochure (see References for details). In fact, Savery, Chin and Yerubandi (2008) cautiously note that, "because the structure of the transformed stress terms is extremely complicated, the transient integration method used is explicit in time." Thus, the present research sought alternative but rigorous methods to track problems in which multiple fluid interfaces existed and for which the dynamics associated with each interface, e.g., mixing zone details azimuthally around the pipe, were also required in detail.

The two-phase model described in an illustrative example later is given for presentation clarity only. We have developed the method for multiple fluids, in fact, any number of non-Newtonian fluids pumped according to any time-varying schedule. While we have explained the simpler two-phase flow behind Equations 9-5-1 and 9-5-2 below, a model attributed to Landau and Lifschitz (1959), a straightforward extension to multiple fluids would require as many concentration equations as there exist contiguous fluid pairs. Such a "brute force" formulation would consist of numerous nonlinearly coupled partial differential equations which, owing to their complexity, also require solution by explicit finite difference time-marching schemes. Because such schemes are by nature unstable numerically, extremely small time steps – and hence, hour-long computing times – would be the rule. This approach would not be conducive to rigsite applications that demand quick solutions and results.

The interface tracking model and diffusion modeling described in this paper is based on a completely different approach. The physical ideas are easily explained. We implicitly assume that all fluid slugs are much longer than the annular diameter; this is easily satisfied in practical operations. Assuming further than interfacial instabilities do not

completely "destroy" the flow, a condition also met by most service companies by virtue of their chemically stable formulations, it is clear that the overall tracking of fluid interfaces depends *only* on the pumping schedule. Thus, interface locations can be predicted from simple "kinematic" analyses requiring straightforward computing programming. Once all interface positions are known, the "dynamics" associated with, say, macroscopic pressure drops, following the slugs, can be obtained from the simulators in Figs. 4a and 4d. If further details related to interfacial diffusive mixing processes are needed, we view the process as one having "boundary layer character" whose properties at left and right are dictated by the macroscopic solution already available. They are *then* computed using Equations 9-5-1 and 9-5-2. Importantly, each on-demand "zoom" request requires the solution of a single concentration equation only and never involves more than one. Thus, the computational approach is fast and stable numerically, offering almost instantaneous feedback, and importantly, operable from standard personal computers at the rigsite. The "plain English" explanation of the solution strategy is now developed in detail. In the next section, we explain the "macroscopic" solution in which interfaces are tracked and how pressures along the borehole wall are computed as functions of time. Then, the detailed boundary layer solution for interface movement and mixing is developed starting on Page 16.

Time-Dependent Pressure Profile in Eccentric Borehole (and at Drill Bit) with Multiple Herschel-Bulkley Fluids Pumped Under General Schedule.

This section discusses the general problem shown in Figure 9-1-1. This is particularly relevant to managed pressure drilling (MPD) and also to cementing operations with combined mud, spacer and cement movement. We will discuss the figure below with regard to MPD operations. Here, multiple fluids (each with its own unique rheological properties) are pumped down the drillpipe following a general pumping schedule. Since different numbers of fluids will occupy the pipe and borehole at different times, with their positions obviously depending on time, it is clear that the pressure distribution along the borehole (and, hence, at the drill bit) will vary with time. The problem we address is the complete pressure solution versus space and time. We note that the drilling system shown in Figure 9-1-1 can be topologically "unwrapped" into the form given in Figure 9-2-1. Hence, we turn to that diagram, which greatly simplifies the discussion (bends introduce centrifugal effects which *are* modeled in the steady simulator).

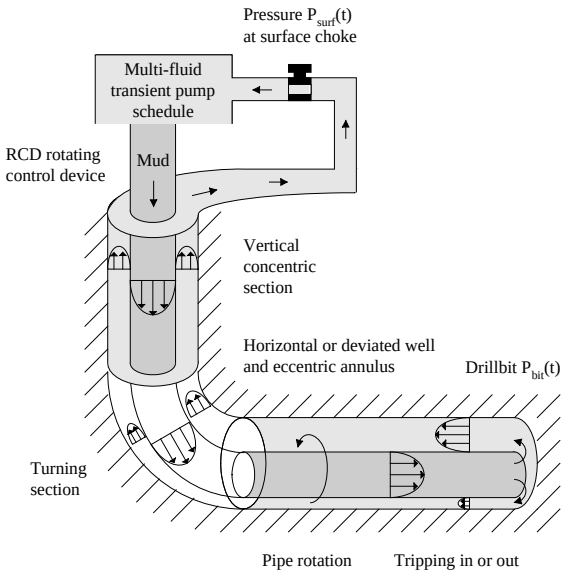

Figure 9-1-1. General managed pressure drilling formulation.

Discussion 9-2. Interface tracking and total pressure drop for multiple fluids pumped in drillpipe and eccentric borehole system.

In this example, we will consider a centered or eccentered drillpipe (with cross-sectional area A_{pipe}) located in a borehole annulus whose geometry is unchanged along its length. The annular area is $A_{annulus}$. Note that while pipe area is simply available from "πR_{pipe}^2," the same is not true for the annulus if the cross-sectional contours from two initially eccentered circles have been edited to incorporate washouts, cuttings beds or fractures. If so, the "Steady 2D" simulator automatically computes and displays total cross-sectional area by summing incremental trapezoidal areas constructed from the curvilinear grid.

Now, mud progresses down the drillpipe, then out through the drillbit, and finally, flows upward in the return annulus. At the outset t = 0, a single initial fluid with Herschel-Bulkley properties (n_0, K_0, $\tau_{0,0}$) is assumed to exist in the pipe and annular system (n is the fluid exponent, K is the consistency factor, and τ_0 is the yield stress). The initial fluid may be flowing or quiescent. At t = 0+, the mud pump starts to act according to a user-defined pumping schedule with piecewise constant rates. At $t = t_0 = 0+$, Fluid "1" with properties (n_1, K_1, $\tau_{0,1}$) is pumped into the pipe at the volume flow rate of Q_1, while at $t = t_1$, a second Fluid "2" with properties (n_2, K_2, $\tau_{0,2}$) is pumped at rate Q_2, and so on. In fact, we have

- Fluid "1" pumped at rate Q_1: $t_0 \le t < t_1$
- Fluid "2" pumped at rate Q_2: $t_1 \le t < t_2$
- Fluid "3" pumped at rate Q_3: $t_2 \le t < t_3$
- Fluid "4" pumped at rate Q_4: $t_3 \le t < t_4$
- Fluid "5" pumped at rate Q_5: $t \ge t_4$

The overall pumping process is illustrated at the top of Figure 9-2-1. Here, fluid introduced at the far right into the

drillpipe travels to the left, and then turns at the drillbit (not shown), and finally progresses to the very far right. The middle diagram shows five interfaces (starting at t_0, t_1, t_2, t_3 and t_4) associated with the onset of each pump actions. The location "z_1" (using the "little z" left-pointing coordinate system shown) describes the interface separating the initial fluid ahead of it with Fluid "1" just behind it. Similarly, "z_2" separates Fluid "1" ahead of it and Fluid "2" behind it. The last Fluid "5" is a single fluid that is pumped continuously without stoppage with flow rate Q_5 for $t \geq t_4$. While more interfaces are easily handled programming-wise, a limit of five (which models six fluid slugs) to enable rapid modeling and job prototyping, was assumed, since this number suffices for most rigsite planning purposes. Once the first interface reaches the end of the drillpipe, shown with length L, that is, $z_1 = L$, it turns into the borehole annulus and travels to the right. Similar descriptions apply to the remaining interfaces. Annular interfaces are described by the "big Z" right-pointing coordinate system at the bottom in Figure 9-2-1. When $Z_1 = L$, the first fluid pumped will have reached the surface.

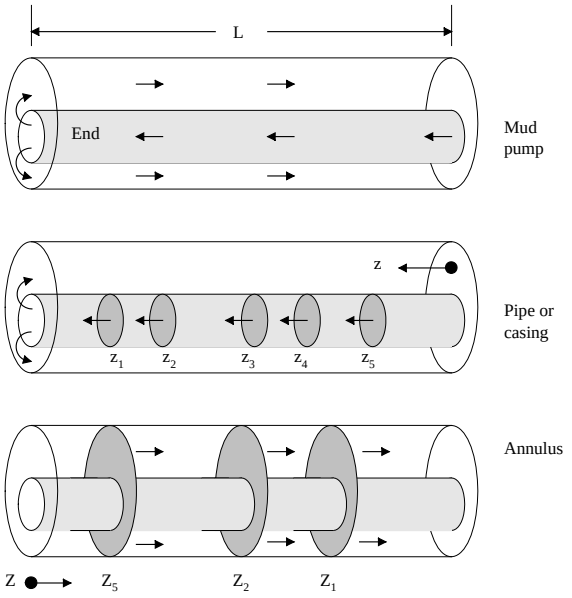

Figure 9-2-1. General pumping schedule.

Figure 9-2-1 provides a "snapshot" obtained for a given instant in time. At different times, the locations of the interfaces will be different, and pressure profiles along the borehole (and hence, at the drillbit) will likewise be different as the Q's also vary. Also, while the discussion focuses on drilling applications with distinct mud interfaces, it is clear that all of the results apply to cement-spacer-mud systems.

Now, we wish to determine the locations of $z_{1,2,3,4,5}$ and $Z_{1,2,3,4,5}$ as functions of time. In general, this is a difficult problem if the fluids are compressible, or if significant mixing is found at fluid interfaces, or both. However, if the lengths of the fluid slugs are long compared to the annular diameter (so that mixing zones are not dynamically significant), and further, if the pump acts instantaneously and transient fluid effects reach equilibrium quickly, interface tracking can be accomplished kinematically. Once the locations of all interfaces are known for any instant in time, pressure drop calculations (for each fluid slug) proceed using the 2D non-Newtonian flow models developed previously.

Two output tables are provided by the "interface tracker." The calculations are performed almost instantaneously by the software model. The two are, respectively, "Drillpipe Fluid Interfaces vs Time" and "Annular Fluid Interfaces vs Time," as shown in Figures 9-2-2 and 9-2-3. The numbers assumed for these tables are obviously not realistic, and for this reason, the units shown in the headings should be ignored for now. They were chosen only so that all results fit on the printed page, with all values allowing convenient visual checking and understanding of the computer output.

ELAPSED TIME		FLOW	Drillpipe Fluid Interface (feet)				
Minutes	Hours	GPMs	z(1)	z(2)	z(3)	z(4)	z(5)
0	0.	1	0	0	0	0	0
1	0.	1	1	0	0	0	0
2	0.	1	2	0	0	0	0
3	0.	1	3	0	0	0	0
4	0.	1	4	0	0	0	0
5	0.	2	5	0	0	0	0
6	0.	2	7	2	0	0	0
7	0.	2	9	4	0	0	0
8	0.	2	11	6	0	0	0
9	0.	2	13	8	0	0	0
10	0.	3	15	10	0	0	0
11	0.	3	18	13	3	0	0
12	0.	3	21	16	6	0	0
13	0.	3	24	19	9	0	0
14	0.	3	27	22	12	0	0
15	0.	4	30	25	15	0	0
16	0.	4	34	29	19	4	0
17	0.	4	38	33	23	8	0
18	0.	4	42	37	27	12	0
19	0.	4	46	41	31	16	0
20	0.	5	50	45	35	20	0
21	0.	5	55	50	40	25	5
22	0.	5	60	55	45	30	10
23	0.	5	65	60	50	35	15
24	0.	5	70	65	55	40	20
25	0.	5	75	70	60	45	25
26	**0.**	**5**	**80**	**75**	**65**	**50**	**30**
27	0.	5	85	80	70	55	35
28	0.	5	90	85	75	60	40
29	0.	5	95	90	80	65	45
30	0.	5	100	95	85	70	50
31	1.	5	0	100	90	75	55
32	1.	5	0	0	95	80	60
33	1.	5	0	0	100	85	65
34	1.	5	0	0	0	90	70
35	1.	5	0	0	0	95	75
36	1.	5	0	0	0	100	80
37	1.	5	0	0	0	0	85
38	1.	5	0	0	0	0	90
39	1.	5	0	0	0	0	95
40	1.	5	0	0	0	0	100
41	1.	5	0	0	0	0	0

Figure 9-2-2. "Drillpipe Fluid Interfaces vs Time."

Note that 0's at early times along a z column indicate absence of the particular fluid in the drillpipe. Also, once the interface has reached the position "100," the end of the borehole in this illustration, the subsequent 0's are no longer meaningful and are used only to populate the table. Also, the very small annular area of $A_{annulus}$ selected later was designed so that we can "watch fluid move" in the table of Figure 9-2-3.

To facilitate visual interpretation, we have assumed that $A_{pipe} = 1$ and $A_{annulus} = 0.5$, so that the nominal linear displacement speeds in the pipe and annulus are $U_{pipe} = Q/A_{pipe}$ and $U_{annulus} = Q/A_{annulus}$. The borehole length is assumed for

clarity to be 100. At the same time, we pump according to the schedule

- Fluid "1" at a rate of $Q_1 = 1$: $0 = t_0 \le t < t_1 = 5$
- Fluid "2" at a rate of $Q_2 = 2$: $5 = t_1 \le t < t_2 = 10$
- Fluid "3" at a rate of $Q_3 = 3$: $10 = t_2 \le t < t_3 = 15$
- Fluid "4" at a rate of $Q_4 = 4$: $15 = t_3 \le t < t_4 = 20$
- Fluid "5" at a rate of $Q_5 = 5$: $t \ge t_4 = 20$

where the five interfaces originate at t_0, t_1, t_2, t_3 and t_4. We next explain Figure 9-2-2. The left column provides elapsed minutes, while the second provides elapsed hours. The volume flow rate is given in the third column. The corresponding drillpipe fluid interfaces $z_{1,2,3,4,5}$ are given in the five remaining columns. Also, each change is flow rate (associated with a new interface) is separated by a single horizontal line spacing to enhance clarity. Consider the result for z_1. In the first time block with $U_{pipe} = 1/1 = 1$, the interface advances at a rate of "1." In the second block with $U_{pipe} = 2/1$, the interfaces advances at the rate "2." As time increases, the easily recognized rate increments are 3, 4 and 5 following the above pump schedule.

ELAPSED TIME		FLOW	Annular Fluid Interface (feet)				
Minutes	Hours	GPMs	z(5)	z(4)	z(3)	z(2)	z(1)
0	0.	1	0	0	0	0	0
1	0.	1	0	0	0	0	0
2	0.	1	0	0	0	0	0
3	0.	1	0	0	0	0	0
4	0.	1	0	0	0	0	0
5	0.	2	0	0	0	0	0
6	0.	2	0	0	0	0	0
7	0.	2	0	0	0	0	0
8	0.	2	0	0	0	0	0
9	0.	2	0	0	0	0	0
10	0.	3	0	0	0	0	0
11	0.	3	0	0	0	0	0
12	0.	3	0	0	0	0	0
13	0.	3	0	0	0	0	0
14	0.	3	0	0	0	0	0
15	0.	4	0	0	0	0	0
16	0.	4	0	0	0	0	0
17	0.	4	0	0	0	0	0
18	0.	4	0	0	0	0	0
19	0.	4	0	0	0	0	0
20	0.	5	0	0	0	0	0
21	0.	5	0	0	0	0	0
22	0.	5	0	0	0	0	0
23	0.	5	0	0	0	0	0
24	0.	5	0	0	0	0	0
25	0.	5	0	0	0	0	0
26	**0.**	**5**	**0**	**0**	**0**	**0**	**0**
27	0.	5	0	0	0	0	0
28	0.	5	0	0	0	0	0
29	0.	5	0	0	0	0	0
30	0.	5	0	0	0	0	0
31	1.	5	0	0	0	0	10
32	1.	5	0	0	0	10	20
33	1.	5	0	0	0	20	30
34	1.	5	0	0	10	30	40
35	1.	5	0	0	20	40	50
36	**1.**	**5**	**0**	**0**	**30**	**50**	**60**
37	1.	5	0	10	40	60	70
38	1.	5	0	20	50	70	80
39	1.	5	0	30	60	80	90
40	1.	5	0	40	70	90	100
41	1.	5	10	50	80	100	0
42	1.	5	20	60	90	0	0
43	1.	5	30	70	100	0	0
44	1.	5	40	80	0	0	0
45	1.	5	50	90	0	0	0
46	1.	5	60	100	0	0	0
47	1.	5	70	0	0	0	0
48	1.	5	80	0	0	0	0
49	1.	5	90	0	0	0	0
50	1.	5	100	0	0	0	0
51	1.	5	0	0	0	0	0

Figure 9-2-3. "Annular Fluid Interfaces vs Time."

The z_1 interface starts moving at t = 0. Now we turn to the second interface and study the column for z_2 results. At t = 5, the second interface starts moving. Because we are already in the second time block, the interface moves at the rate "2." Subsequent speeds are 3, 4 and 5. Similarly, z_3 starts at t = 10 and rate increments with 3, followed by 4 and 5, and so on. We have described Figure 9-2-2 from the perspective of tracking individual fronts. However, the table is important for pressure calculations. Let us consider the results obtained at t = 26 (these are shown in bold font for emphasis). In particular, we have

ELAPSED TIME		FLOW	Drillpipe Fluid Interface (feet)				
Minutes	Hours	GPMs	z(1)	z(2)	z(3)	z(4)	z(5)
26	**0.**	**5**	**80**	**75**	**65**	**50**	**30**

This printout indicates that, at t = 26, the front z_1 is located at z = 80, while the last front z_5 is located at z = 30. The drillpipe thus contains six distinct fluid slugs at $100 > z > 80$, $80 > z > 75$, $75 > z > 65$, $65 > z > 50$, $50 > z > 30$ and $30 > z > 0$ where "100" refers to the assumed borehole length. In fact –

$100 > z > 80$ contains "initial fluid" with properties (n_0, K_0, $\tau_{0,0}$)
$80 > z > 75$ contains Fluid "1" with properties (n_1, K_1, $\tau_{0,1}$)
$75 > z > 65$ contains Fluid "2" with properties (n_2, K_2, $\tau_{0,2}$)
$65 > z > 50$ contains Fluid "3" with properties (n_3, K_3, $\tau_{0,3}$)
$50 > z > 30$ contains Fluid "4" with properties (n_4, K_4, $\tau_{0,4}$)
$30 > z > 0$ contains Fluid "5" with properties (n_5, K_5, $\tau_{0,5}$)

If a non-Newtonian flow model for a Herschel-Bulkley fluid in a circular pipe were available that gave the pressure gradient $(\partial P/\partial z)_{pipe,n}$ for any of the given fluid slugs "n" flowing at rate Q with a pipe radius $(A_{pipe}/\pi)^{1/2}$, then the total drillpipe pressure drop is simply calculated from $(100 - 80)\ (\partial P/\partial z)_{pipe,0} + (80 - 75)\ (\partial P/\partial z)_{pipe,1} + (75 - 65)\ (\partial P/\partial z)_{pipe,2} + (65\text{-}50)\ (\partial P/\partial z)_{pipe,3} + (50 - 30)\ (\partial P/\partial z)_{pipe,4} + (30 - 0)\ (\partial P/\partial z)_{pipe,5}$. The flow rate Q used would be the one applicable at the time the snapshot was taken, in this case, Q = 5 at t = 26 (a single rate applies to all slugs at any instant in time). Now, at time t = 26, Figure 9-2-3 shows, as indicated by "0's," that none of the pumped fluids have arrived in the annulus, that is, we have –

ELAPSED TIME		FLOW	Annular Fluid Interface (feet)				
Minutes	Hours	GPMs	Z(5)	Z(4)	Z(3)	Z(2)	Z(1)
26	**0.**	**5**	**0**	**0**	**0**	**0**	**0**

Thus, the only fluid residing in the annulus is the initial fluid. If the pressure gradient obtained from an eccentric flow analysis is $(\partial P/\partial z)_{annulus,0}$, then the pressure drop in the annulus is just $(100 - 0)\ (\partial P/\partial z)_{annulus,0}$. If we further denote by Δ the pressure drop through the drillbit, then the total pressure drop through the entire pipe-bit-annulus system is obtained by summing the prior three results, that is, $(100 - 80)\ (\partial P/\partial z)_{pipe,0} + (80 - 75)\ (\partial P/\partial z)_{pipe,1} + (75 - 65)\ (\partial P/\partial z)_{pipe,2} + (65\text{-}50)\ (\partial P/\partial z)_{pipe,3} + (50 - 30)\ (\partial P/\partial z)_{pipe,4} + (30 - 0)\ (\partial P/\partial z)_{pipe,5} + \Delta + (100 - 0)\ (\partial P/\partial z)_{annulus,0}$, which is the pressure (additive to the surface choke pressure P_{SURF}) required at the mud pump to support this multi-slug flow.

The software that creates Figure 9-2-2 also provides the times at which fluid interfaces in the drillpipe enter the borehole annulus. These are obtained from the table in Figure 9-2-2 by noting the "100" marker. In this case, we have

```
Borehole total length L, is:     100 ft.
Fluid "1" enters annulus at:      30 min.
Fluid "2" enters annulus at:      31 min.
Fluid "3" enters annulus at:      33 min.
Fluid "4" enters annulus at:      36 min.
Fluid "5" enters annulus at:      40 min.
```

We next consider another time frame, say t = 36, for which the drillpipe interfaces have entered the annulus, and explain how annular pressure drops are determined, e.g., see Figure 9-2-4. For this time frame, Figure 9-2-3 gives

ELAPSED TIME		FLOW	Annular Fluid Interface (feet)				
Minutes	Hours	GPMs	Z(5)	Z(4)	Z(3)	Z(2)	Z(1)
36	1.	5	0	0	30	50	60

This indicates that three interfaces exist in the annulus, with Z_1 located at the far right Z = 60, followed by Z_2 at Z = 50 and Z_3 at Z = 30. Since the fluid ahead of Z_1 is the "initial fluid," the total annular pressure drop is calculated from the sum (100 – 60) $(\partial P/\partial z)_{annulus,0}$ + (60 – 50) $(\partial P/\partial z)_{annulus,1}$ + (50 – 30) $(\partial P/\partial z)_{annulus,2}$ + (30 – 0) $(\partial P/\partial z)_{annulus,3}$ where subscripts denote fluid type for the annular model.

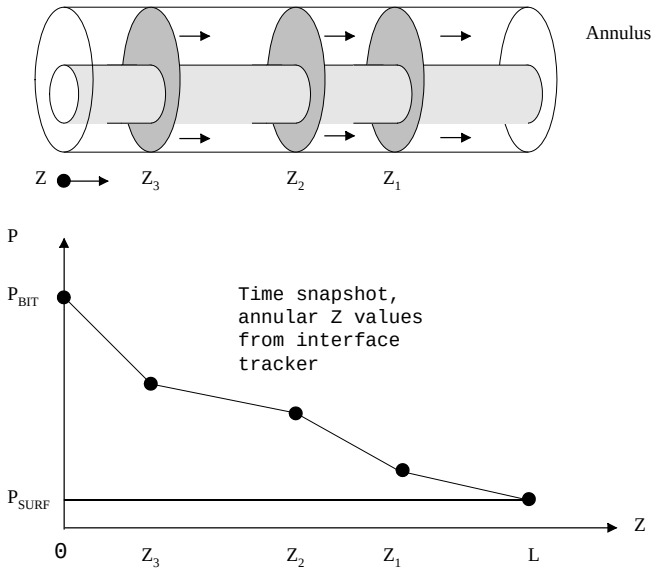

Figure 9-2-4. Example annular interface distribution.

We note that the actual pressure P_{BIT} at the drillbit *in the formation* is obtained by adding the total annular pressure drop to the pressure P_{SURF} obtained at the surface choke. The value of P_{SURF} is in itself a "boundary condition," and, importantly, the pressure P_{BIT} at the bottom of the annulus *in the formation* does not depend on the pressure drop Δ through the drillbit. On the other hand, the pressure required at the pump to move the system flow includes pipe, bit and annular losses, as shown in Figure 9-2-5 for one interface configuration.

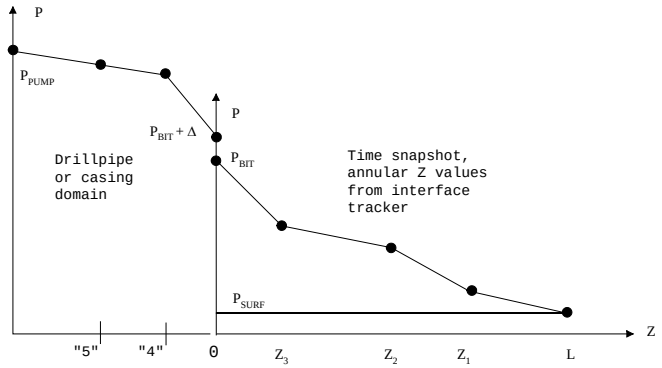

Figure 9-2-5. Complete drillpipe-drillbit-annulus system.

THREE-DIMENSIONAL, TRANSIENT, MULTIPHASE INTERFACIAL FLOW ANALYSIS

Let us recall that, for purely steady, two-dimensional, non-rotating, single-phase flow of a yield-stress or non-yield non-Newtonian fluid, the general partial differential equation below applies.

$$\partial\,(N\,\partial u/\partial y)/\,\partial y \;+\partial\,(N\,\partial u/\partial x)/\,\partial x \;=\partial P/\partial z \qquad (4)$$

We again emphasize that the above equation can be easily solved in seconds for highly eccentric annuli with or without axial pipe movement, using methods based on boundary-conforming curvilinear coordinates, with either pressure gradient or volume flow rate specified, via the software implementation in Fig. 4a.

When the inner pipe rotates, the method of Fig. 4a does not apply, since the numerical solution of a purely steady formulation is unstable. Again, this does not mean that steady solutions with rotation are not possible. As demonstrated in a companion work on the effect of rotation on flowrate and pressure gradient in eccentric holes, steady, rotating flow solutions can be easily obtained as the large-time asymptotic solution of a transient formulation. This is accomplished using the code in Fig. 4d, which solves the coupled, single-phase, momentum equations in the axial and azimuthal directions on curvilinear grids, again for extended Herschel-Bulkley fluids, with or without axial pipe movement. The solution process requires seconds for low-density fluids, but for fluids denser than water, may require 2-3 minutes of computing time.

For the remainder of this paper, we will therefore assume that the axial pressure gradient on a single-phase flow basis is readily available for inner pipe that is moving both axially and azimuthally using the formulations in Fig. 4a or Fig. 4d. These pressure gradients, as we will see, provide the auxiliary conditions needed in the formulation and solution of the general transient, multiphase flow formulation in three spatial dimensions.

In the approach to the general problem for multiple slugs of non-Newtonian fluid pumped into the annulus following a general pumping schedule, we decompose the formulation into two parts. We implicitly assume that each slug of fluid is very

long compared to the annular diameter. Thus, the macroscopic motion and position of all fluid interfaces can be approximately determined by the interface tracking model that we had developed earlier. Again, the model tracks more than interface positions versus time: the complete pressure profile along the borehole is available as a function of time. This therefore includes the time history of pressure at the drillbit, an important consideration for managed pressure drilling.

To obtain interfacial properties related to diffusive and convective mixing, we adopt the "boundary layer" strategy used in fluid mechanics. In flows past airplane wings, for instance, the pressure field is first determined on an inviscid flow basis; this pressure is then "impressed" across the boundary layer at the wing surface and local frictional effects satisfying a diffusion equation are then calculated.

For this problem, the interface tracking model provides the macroscopic description, one which dictates where interfaces are, and then, by applying the methods of Fig. 4a and Fig. 4d, additionally determines overall pressure histories at each location along the borehole. Now, the microscopic "boundary layer" formulation is one seeking to determine the details of the convective-diffusive mixing process in a relatively narrow zone. Unlike an aircraft boundary layer, the transition zone or mixing region here can be several feet. As in boundary layer theory, we now "zoom" into the nearfield adjacent to the interface separating two contiguous fluids, as shown in Figure 9-5-1, in a three-dimensional sense. We refer to this as the "Zoom3D" function.

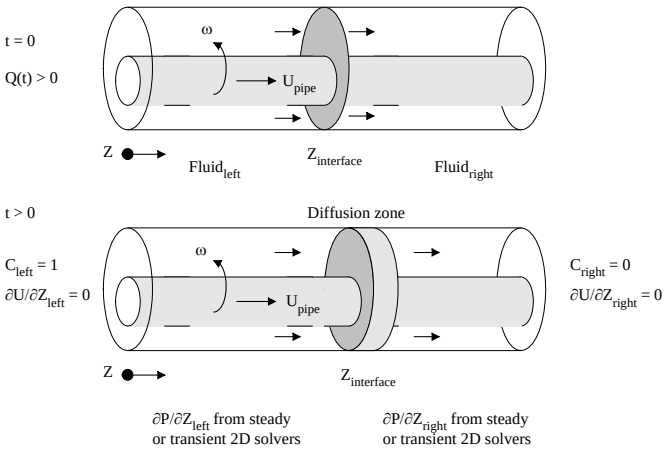

Figure 9-5-1. Transient, multiphase, boundary layer model.

The top diagram in Figure 9-5-1 shows a "left" fluid displacing a "right" fluid at t = 0. The interface, per the interface tracking model, is infinitesimally thin. At later times t > 0, the diagram at the bottom applies, indicating a widened mixing zone. In the nearfield model, we ask how long the zone takes to widen and its corresponding width, which may vary across the cross-section of the annulus, and also as a function of time. The extent of multiphase fluid mixing dictates the quality in a cementing job. The multiphase problem, we might note, is not so important to drilling, but other features of the three-dimensional method may be useful in real-world drilling applications.

Mathematical formulation. Evidently, the annular flow problem is now three-dimensional, transient and multiphase. How is this modeled and solved? We obtain practical solutions following the approach first suggested by Landau and Lifschitz (1959), although modified to account for the complexities of the problem at hand. Instead of Eq. 4, we now have the transient axial momentum law in Equation 9-5-1, in which we have added a third flow direction "z" oriented axially. The left side represents nonlinear convective acceleration effects, with "v" being the azimuthal velocity function. N(C) now represents a concentration-dependent apparent viscosity function, while the pressure gradient $\partial P/\partial z$ now varies in the z direction in a manner to be discussed. Note that the equation for "v" is similar to Equation 9-5-1.

The concentration C(x,y,z,t) satisfies the convective diffusive law in Equation 9-5-2 where ε represents an empirically determined diffusion coefficient that may depend on flow rate, species or concentration (its transformed equivalent is shown in Equation 9-5-3 for reference, noting that the result for "u" takes a similar form). Note that the solutions for u, v and C are now nonlinearly coupled transient partial differential equations of parabolic type. Laboratory measurements may be used in one-dimensional experiments to determine ε – then, use of this ε in three-dimensional transient applications may yield important physical insights relating to the role of annular geometry.

$$\rho(\partial u/\partial t + v/r\ \partial u/\partial\theta + u\ \partial u/\partial z) =$$
$$= -\partial P/\partial z + N(C)\ (\partial^2 u/\partial x^2 + \partial^2 u/\partial y^2 + \partial^2 u/\partial z^2) + \ldots \quad (9\text{-}5\text{-}1)$$

$$\partial C/\partial t + v/r\ \partial C/\partial\theta + u\ \partial C/\partial z =$$
$$= -\varepsilon\ (\partial^2 C/\partial x^2 + \partial^2 C/\partial y^2 + \partial^2 C/\partial z^2) \quad (9\text{-}5\text{-}2)$$

$$\partial C/\partial t + \mathbf{q}(\xi, \eta, z) \cdot \nabla C =$$
$$= \varepsilon\ \{C_{zz} + (\alpha C_{\xi\xi} - 2\beta C_{\xi\eta} + \gamma C_{\eta\eta})/J^2\} \quad (9\text{-}5\text{-}3)$$

Solution strategy. As in previous work, the differential operators in the x-y cross-space are re-expressed in curvilinear coordinates, while "z" remains "as is." Central differences are used for all spatial derivatives and backward differences are used for time derivatives in an explicit marching scheme. The boundary conditions are shown in Figure 9-5-1. Far upstream and far downstream, the velocity field is assumed to be smooth with $\partial u/\partial z = 0$. At the left, a "left fluid" is assumed with a concentration C = 1, while at the right, a second "right fluid" is taken with C = 0. The initial condition is shown at the top of Figure 9-5-1. At each time step, the spatial distribution of C is monitored. The front defined by the locus of points for which C = 1 travels to the right. To its left, the pressure gradient $(\partial P/\partial z)_{left}$ obtained from the model in Fig. 4a or Fig. 4d is used accordingly as the pipe does not or does rotate. Similarly, the pressure gradient $(\partial P/\partial z)_{right}$ is used at the right of the interface. In a uniform fluid, the pressure gradient is constant throughout. When two contiguous slugs of fluid move at a flow rate Q, two different pressure gradients are present, since two different rheologies are present in the problem. Note that, because slug lengths are great compared

to annular diameters, only two fluids (satisfying a single concentration equation) need to be treated at any given "Zoom3D" application, in contrast to the earlier work reported by the first author and his colleagues.

Example results. In the numerical model, we have allowed variations in borehole annular geometry in the axial direction. This is important in practical applications where the effects of anomalies like localized washouts and cuttings accumulations on velocities and viscous stresses are to be studied. Thus, in order to support three-dimensional modeling, the cross-sectional mappings are performed as needed, with transformations Jacobians and other metrics incorporated into three-dimensional arrays.

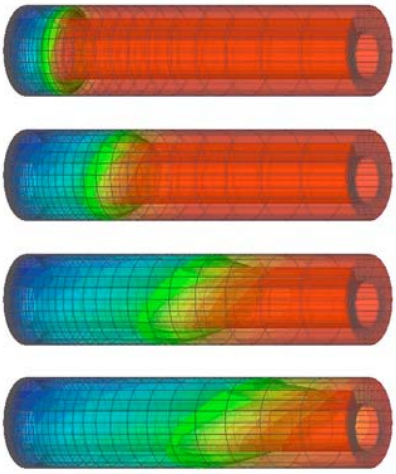

Figure 9-5-2. Uniform eccentric annulus.

Figure 9-5-2 shows the computed concentration field as a function of time, with the fluid interface propagating to the right and widening as it moves. Here, high velocities are seen at the wide side of the annulus. The amount of diffusion clearly differs azimuthally around the pipe. The annular region is clearly eccentric, but the borehole cross-section does not change with axial position. In Figure 9-5-3, we have a concentric annulus, however a highly eccentric section is introduced between the borehole ends in order to demonstrate three-dimensional effects and computational stability in the presence of sudden geometric changes. Figure 9-5-4 displays typical results from Savery, Tonmukayakul, Chin *et al* (2008) which support the approach used in this paper. Note that while we have plotted the concentration field as it varies with time, in order to highlight cement-mud displacement operations, we could easily have plotted the axial velocity field using color coded graphics for single-phase flow drilling applications. For horizontal drilling, the ability to model local geometric anomalies, e.g., cuttings beds, washouts, and so on, supports well stability and hole cleaning planning activities.

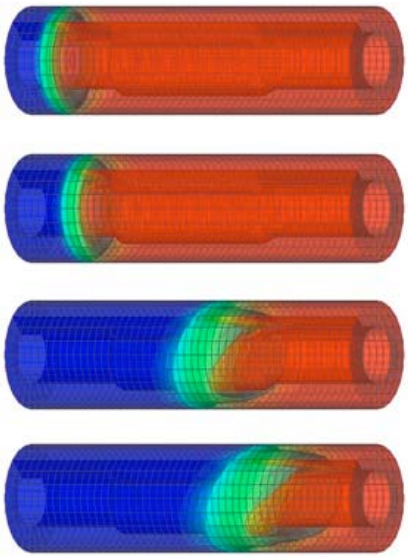

Figure 9-5-3. Concentric annulus with embedded eccentric section.

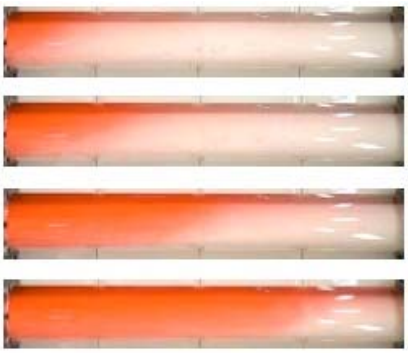

Figure 9-5-4. Experimental results, Savery, Tonmukayakul, Chin *et al* (2008).

User interface. As noted, e.g., refer to the formulation outlined in Figure 9-5-1, for general non-Newtonian flows with pipe rotation, inputs to multiphase calculations include pressure gradients obtained from the detailed calculations in Fig. 4a and 4d. User interface design is complicated by these auxiliary requirements and the aim is an easy-to-use software environment that solves this near-field problem as well as the macroscopic interface tracking automatically. In order to be completely transparent to the user, the interface logic must be capable of detecting slow convergence (or non-convergence) and correct for this without human intervention. This is presently an area of active work. While important, the task is straightforward and involves programming only. For Newtonian mixtures, the availability of exact scaling laws automates the computations. The interface in Figure 9-5-5, for example, allows introduction of borehole anomalies in the geometry definition with online editing, and also, provides "on demand" movie playback of all physical properties in addition to detailed tabulations. The menus in Figures 4a, 4d and 9-5-5 are called from a central menu. The complete system will integrate all of these software elements.

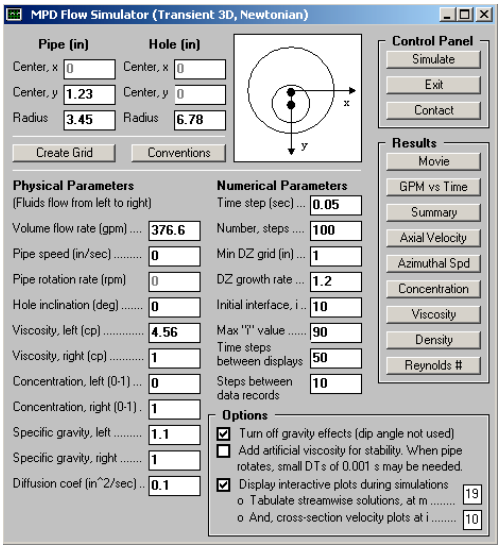

Figure 9-5-5. Candidate multiphase flow user interface.

More general problems. An additional, more general, two-part interface has been developed for non-Newtonian flow problems with or without rotation. This is accessed from the high-level menu of Fig. 9-5-6. The first menu is shown in the foreground of Fig. 9-5-7 and accepts inputs related to the pumping schedule and the fluid rheologies associated with each pump interval. For example, two distinct pressure gradients would be inputted to model the displacement of one fluid by another. The second menu is shown in the background and accepts inputs related to annular geometry definition and simulaton parameters.

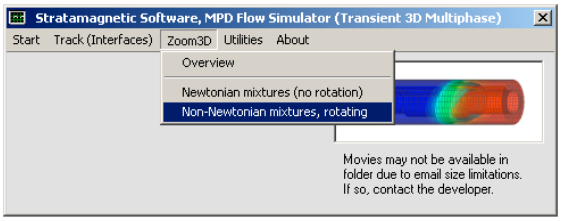

Figure 9-5-6. High level transient, 3D, multiphase menu.

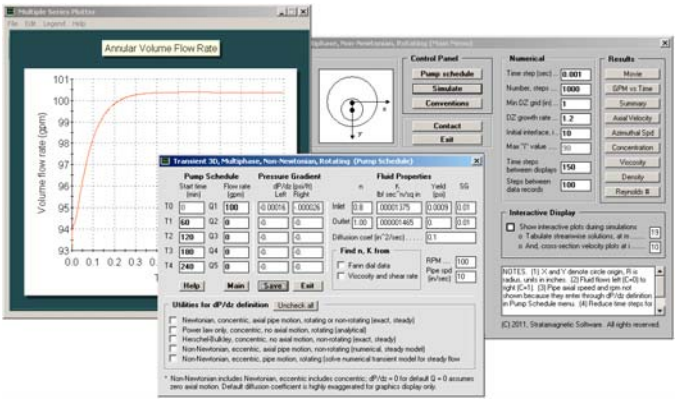

Figure 9-5-7. Transient, 3D, two-phase mixture formulation.

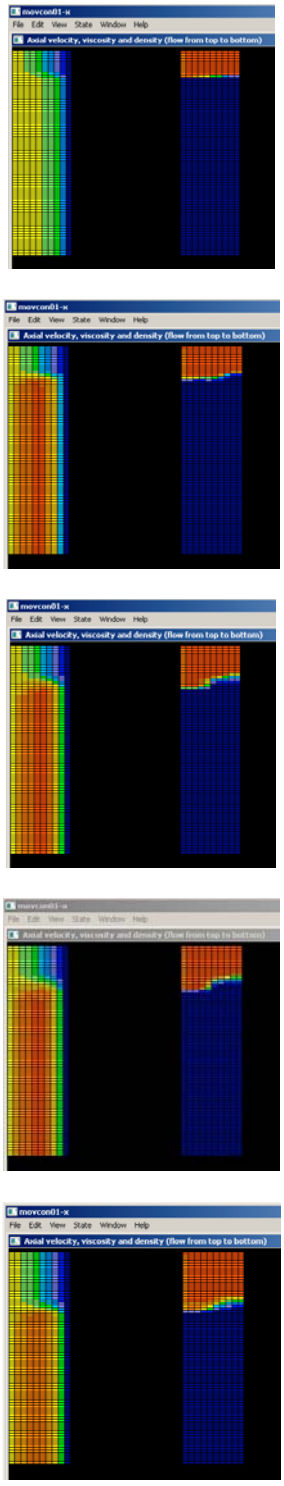

Figure 9-5-8. Axial velocity (left), apparent viscosity (right), flow moving downward in each frame, time increases downward from frame to frame.

Ans-Vis-X.dat - Notepad

File Edit Format View Help

Time (sec): 9.0

I:	1	2	3	4	5	6	7
1	0.997E+02	0.913E+02	0.913E+02	0.913E+02	0.913E+02	0.913E+02	0.913E+02
2	0.101E+03	0.943E+02	0.943E+02	0.943E+02	0.943E+02	0.943E+02	0.943E+02
3	0.101E+03	0.996E+02	0.996E+02	0.996E+02	0.996E+02	0.996E+02	0.996E+02
4	0.101E+03	0.100E+03	0.100E+03	0.100E+03	0.100E+03	0.100E+03	0.100E+03
5	0.101E+03	0.100E+03	0.100E+03	0.100E+03	0.100E+03	0.100E+03	0.100E+03
6	0.101E+03	0.101E+03	0.101E+03	0.101E+03	0.101E+03	0.101E+03	0.101E+03
7	0.101E+03	0.101E+03	0.101E+03	0.101E+03	0.101E+03	0.101E+03	0.101E+03
8	0.101E+03	0.101E+03	0.101E+03	0.101E+03	0.101E+03	0.101E+03	0.101E+03
9	0.101E+03	0.101E+03	0.101E+03	0.101E+03	0.101E+03	0.101E+03	0.101E+03
10	0.101E+03	0.101E+03	0.101E+03	0.101E+03	0.101E+03	0.101E+03	0.101E+03
11	0.101E+03	0.101E+03	0.101E+03	0.101E+03	0.101E+03	0.101E+03	0.101E+03

Ans-Vis-X.dat - Notepad

File Edit Format View Help

87	88	89	90
0.100E+02	0.100E+02	0.100E+02	0.100E+02
0.100E+02	0.100E+02	0.100E+02	0.100E+02
0.100E+02	0.100E+02	0.100E+02	0.100E+02
0.100E+02	0.100E+02	0.100E+02	0.100E+02
0.100E+02	0.100E+02	0.100E+02	0.100E+02
0.100E+02	0.100E+02	0.100E+02	0.100E+02
0.100E+02	0.100E+02	0.100E+02	0.100E+02
0.100E+02	0.100E+02	0.100E+02	0.100E+02
0.100E+02	0.100E+02	0.100E+02	0.100E+02
0.100E+02	0.100E+02	0.100E+02	0.100E+02
0.100E+02	0.100E+02	0.100E+02	0.100E+02

Figure 9-5-9. Apparent viscosity for "constant m" or azimuthal angle.

Ans-Usp-X.dat - Notepad

File Edit Format View Help

Time (sec): 9.0

I:	1	2	3	4	5	6	7
1	10.000	10.000	10.000	10.000	10.000	10.000	10.000
2	9.464	9.464	9.464	9.464	9.464	9.464	9.464
3	8.865	8.865	8.865	8.865	8.865	8.865	8.865
4	8.198	8.198	8.198	8.198	8.198	8.198	8.198
5	7.454	7.454	7.454	7.454	7.454	7.454	7.454
6	6.616	6.616	6.616	6.616	6.616	6.616	6.616
7	5.663	5.663	5.663	5.663	5.663	5.663	5.663
8	4.567	4.567	4.567	4.567	4.567	4.567	4.567
9	3.291	3.291	3.291	3.291	3.291	3.291	3.291
10	1.788	1.788	1.788	1.788	1.788	1.788	1.788
11	0.000	0.000	0.000	0.000	0.000	0.000	0.000

Ans-Usp-X.dat - Notepad

File Edit Format View Help

84	85	86	87	88	89	90
10.000	10.000	10.000	10.000	10.000	10.000	10.000
11.700	11.700	11.700	11.700	11.700	11.700	11.700
12.930	12.930	12.930	12.930	12.930	12.930	12.930
13.756	13.756	13.756	13.756	13.756	13.756	13.756
14.222	14.222	14.222	14.222	14.222	14.222	14.222
14.327	14.327	14.327	14.327	14.327	14.327	14.327
13.973	13.973	13.973	13.973	13.973	13.973	13.973
12.930	12.930	12.930	12.930	12.930	12.930	12.930
10.755	10.755	10.755	10.755	10.755	10.755	10.755
6.743	6.743	6.743	6.743	6.743	6.743	6.743
0.000	0.000	0.000	0.000	0.000	0.000	0.000

Figure 9-5-10. Axial velocity solution.

Ans-Vth-X.dat - Notepad

File Edit Format View Help

Time (sec): 9.0

I:	1	2	3	4	5	6	7
1	0.314E+02	0.314E+02	0.314E+02	0.314E+02	0.314E+02	0.314E+02	0.314E+02
2	0.277E+02	0.277E+02	0.277E+02	0.277E+02	0.277E+02	0.277E+02	0.277E+02
3	0.242E+02	0.242E+02	0.242E+02	0.242E+02	0.242E+02	0.242E+02	0.242E+02
4	0.208E+02	0.208E+02	0.208E+02	0.208E+02	0.208E+02	0.208E+02	0.208E+02
5	0.176E+02	0.176E+02	0.176E+02	0.176E+02	0.176E+02	0.176E+02	0.176E+02
6	0.145E+02	0.145E+02	0.145E+02	0.145E+02	0.145E+02	0.145E+02	0.145E+02
7	0.114E+02	0.114E+02	0.114E+02	0.114E+02	0.114E+02	0.114E+02	0.114E+02
8	0.851E+01	0.851E+01	0.851E+01	0.851E+01	0.851E+01	0.851E+01	0.851E+01
9	0.564E+01	0.564E+01	0.564E+01	0.564E+01	0.564E+01	0.564E+01	0.564E+01
10	0.281E+01	0.281E+01	0.281E+01	0.281E+01	0.281E+01	0.281E+01	0.281E+01
11	0.000E+00	0.000E+00	0.000E+00	0.000E+00	0.000E+00	0.000E+00	0.000E+00

Figure 9-5-11. Azimuthal velocity.

Ans-Rey-X.dat - Notepad

File Edit Format View Help

Time (sec): 9.0

I:	1	2	3	4	5	6	7
1	0.192E+01	0.209E+01	0.209E+01	0.209E+01	0.209E+01	0.209E+01	0.209E+01
2	0.180E+01	0.192E+01	0.192E+01	0.192E+01	0.192E+01	0.192E+01	0.192E+01
3	0.168E+01	0.170E+01	0.170E+01	0.170E+01	0.170E+01	0.170E+01	0.170E+01
4	0.156E+01	0.156E+01	0.156E+01	0.156E+01	0.156E+01	0.156E+01	0.156E+01
5	0.141E+01	0.142E+01	0.142E+01	0.142E+01	0.142E+01	0.142E+01	0.142E+01
6	0.125E+01	0.126E+01	0.126E+01	0.126E+01	0.126E+01	0.126E+01	0.126E+01
7	0.107E+01	0.107E+01	0.107E+01	0.107E+01	0.107E+01	0.107E+01	0.107E+01
8	0.866E+00	0.864E+00	0.864E+00	0.864E+00	0.864E+00	0.864E+00	0.864E+00
9	0.624E+00	0.622E+00	0.622E+00	0.622E+00	0.622E+00	0.622E+00	0.622E+00
10	0.339E+00	0.338E+00	0.338E+00	0.338E+00	0.338E+00	0.338E+00	0.338E+00
11	0.000E+00	0.000E+00	0.000E+00	0.000E+00	0.000E+00	0.000E+00	0.000E+00

Figure 9-5-12. Reynolds number, very low, stable flow.

On completion of the transient, three-dimensional, multiphase simulation, different types of outputs are available. For instance, Figure 9-5-8 captures movie frames showing the timewise evolution of the velocity and apparent viscosity fields in an azimuthal plane specified by the user. Movies are accessed by clicking the "Movie" button in Figure 9-5-7. The same menu also provides direct access to numbers, and typical screens are shown in Figures 9-5-9 to 9-5-12. Note that the very low Reynolds numbers shown in the last printout indicate fluid stability on a single-phase flow basis. The fluid interface in the above movie frames is seen to widen gradually as it convects downward.

Closing Remarks

The present paper describes new capabilities in modeling steady and transient non-Newtonian flow in highly eccentric annuli, with or without plug zones associated with yield stress fluids, with realistic geometric anomalies, plus effects like borehole axis curvature and drillpipe translation and rotation. In particular, we address the flow of multiple slugs of non-Newtonian fluid pumped into the pipe and eccentric annulus system, and in doing so, track all interfaces, borehole pressure profiles, plus details of interfacial mixing processes. The rigorous fluid-dynamical model formulated here and its exact mathematical solution, augmented by rapidly converging algorithms and convenient color displays, are intended to provide state-of-the-art capabilities useful to managed pressure drilling, hole cleaning and cement-mud displacement in highly deviated and horizontal wells.

Acknowledgments

The authors gratefully acknowledge 2009-2011 support from the United States Department of Energy for their technical proposal "Advanced Steady-State and Transient, Three-Dimensional, Single and Multiphase, Non-Newtonian Simulation System for Managed Pressure Drilling." This effort was administered by the Research Partnership to Secure Energy for America (RPSEA) through its Ultra-Deepwater Program under Subcontract No. 08121-2502-01. The curvilinear grid generation research was also supported by the United States Department of Energy, in particular, under Small Business Innovation Research Grant DE-FG03-99ER82895 in 1999-2000. We are indebted to Art Schroeder, Energy Valley, to Jim Chitwood, Chevron, and to James Pappas, RPSEA, for their encouragement and advice, and especially to John Lofton, Chevron, for his engineering insights and guidance related to several areas in the modeling of rotating pipe flow effects. The views expressed in this paper represent those of the authors only and not necessarily the opinions of any program sponsors.

References

1. Becker, T.E., Morgan, R.G., Chin, W.C. and Griffith, J.E., "Improved Rheology Model and Hydraulics Analysis for Tomorrow's Wellbore Fluid Applications," SPE Paper No. 82415, presented at the SPE Production and Operations Smposium, Oklahoma City, OK, 23-25 March 2003.
2. Chin, W.C., Borehole Flow Modeling in Horizontal, Deviated and Vertical Wells, Gulf Publishing, Houston, 1992.
3. Chin, W.C., Computational Rheology for Pipeline and Annular Flow, Elsevier, Cambridge, 2001.
4. Chin, W.C., Quantitative Methods in Reservoir Engineering, Elsevier, Cambridge, 2002.
5. Chin, W.C. and Zhuang, X., "Exact Non-Newtonian Flow Analysis of Yield Stress Fluids in Highly Eccentric Borehole Annuli with Pipe or Casing Translation and Rotation," SPE 131234-PP, presented at the CPS/SPE International Oil & Gas Conference and Exhibition, Beijing, China, 8-10 June 2010.
6. Deawwanich, T., Liew, J.C., Nguyen, Q.D., Savery, M., Tonmukayakul, N. and Chin, W.C., "Displacement of Viscoplastic Fluids in Eccentric Annuli: Numerical Simulation and Experimental Validation," *Chemeca 2008 Conference*, Newcastle, Australia, Sept. 28 - Oct. 1, 2008.
7. Halliburton Energy Services, "Displace 3D™ Simulator," Product Brochure H06210, 2008.
8. Landau, L.D. and Lifschitz, E.M., Fluid Mechanics, Pergamon Press, London, 1959.
9. Nguyen, Q.D., Deawwanich, T., Tonmukayakul, N., Savery, M.R. and Chin, W.C., "Flow Visualization and Numerical Simulation of Viscoplastic Fluid Displacements in Eccentric Annuli," *XVth International Congress on Rheology (ICR 2008)*, Society of Rheology 80th Annual Meeting, Monterey, CA, Aug. 3-8, 2008.
10. Savery, M., Chin, W.C. and Babu Yerubandi, K., "Modeling Cement Placement Using a New Three-Dimensional Flow Simulator," Paper AADE-08-DF-HO-08, 2008 AADE Fluids Conference and Exhibition, American Association of Drilling Engineers, Houston, Texas, April 8-9, 2008.
11. Savery, M., Darbe, R. and Chin, W.C., "Modeling Fluid Interfaces During Cementing Using a Three-Dimensional Mud Displacement Simulator," OTC Paper 18513, *2007 Offshore Technology Conference (OTC)*, April 30 – May 3, 2007, Houston, TX
12. Savery, M., Tonmukayakul, P., Chin, W.C., Deawwanich, T., Liew, J. and Q. D. Nguyen, "Laminar Displacement of Viscoplastic Fluids in Eccentric Annuli – Numerical Simulation and Experimental Validations," *XXII International Congress of Theoretical and Applied Mechanics (ICTAM 2008)*, Adelaide, Australia, Aug. 24-29, 2008.
13. Souza Mendes, P.R. and Dutra, E.S.S., "A Viscosity Function for Viscoplastic Liquids," Annual Transactions of the Nordic Rheology Society, Vol. 12, 2004.